Journal of Physiology (1993), **471**, *pp.* 129–157
With 9 figures
Printed in Great Britain

SPACE AND TIME CHARACTERISTICS OF TRANSMITTER RELEASE AT THE NERVE–ELECTROPLAQUE JUNCTION OF *TORPEDO*

BY ROMAIN GIROD, PHILIPPE CORRÈGES, JEAN JACQUET AND YVES DUNANT

From the Département de Pharmacologie, Centre Médical Universitaire, 1211 Genève 4, Switzerland

(*Received 10 March 1992*)

SUMMARY

1. A loose patch electrode was used to stimulate axon terminals and to record evoked electroplaque currents (EPCs) in a limited area of innervated membrane of the electric organ of *Torpedo marmorata*. Electrophysiological signals were compared to the predictions of a semi-quantitative model of synaptic transmission which was designed to simulate the release of several packets of neurotransmitter molecules, at the same or at different sites of the synapse, synchronously or with various temporal patterns.

2. The amplitude distribution of EPCs evoked by activation of nerve terminals showed quantal steps. The time to peak of EPCs was in most cases independent of amplitude, but in their decaying phase a positive correlation was seen between half-decay time and amplitude. Comparison with the model suggested that (i) a dynamic interaction occurred at the end of the EPC between the fields of postsynaptic membrane activated by individual quanta, and (ii) the sites of quantal release in the electric organ are separated from each other by 600–1000 nm.

3. Spontaneous miniature electroplaque potentials (MEPPs) were recorded externally with the same type of loose patch electrode. The majority (75%) of external MEPPs displayed a homogeneous and rapid time course. This fast MEPP population had a mean time to peak of 0·43 ms, a half-decay time of 0·45 ms and a time constant of decay of 0·35 ms.

4. Despite homogeneous characteristics of time course, fast MEPPs exhibited a wide amplitude distribution with a main population which could be fitted by a Gaussian curve around 1 mV, and another population of small amplitude. Both the time-to-peak and the half-decay time of fast MEPPs showed a positive correlation with the amplitude from the smallest to the largest events. Acetylcholinesterase was not blocked.

5. In addition to the fast MEPPs, spontaneous signals exhibiting a slow rate of rise, or a slow rate of decay, or both were observed. They occurred at any time during the experiment, independently of the overall frequency. Approximately 15% of the total number of events had a slow rise but their decay phase was nevertheless rapid and could be ascribed to the kinetics of receptors. These slow-rising MEPPs exhibited a variety of conformations: slow but smooth rise, sudden change of slope and

sometimes several bumps or inflexions. Their average amplitude was significantly smaller than that of the main population of fast MEPPs.

6. Composite MEPPs with multiple peaks as well as bursts of small MEPPs were often encountered, even during periods of low frequency. They were suggestive of a complete disorganization of quantal events.

7. Fast, slow and composite MEPPs were analysed using the computer model. To simulate the entire variety of signals we had to assume that the MEPPs were generated by either synchronized or desynchronized emission of small quantities of transmitter. The typical relationship observed between amplitude and time course in the population of fast MEPPs suggested that the different amounts of transmitter composing a quantum were delivered synchronously close to each other (either at the same spot or at less than 200 nm apart); it is proposed that they acted on overlapping fields of receptors and that their responses summed up in a superadditive manner.

8. Computer analysis of the slow-rising MEPPs was of particular interest since their rapid decay phase indicated that the postsynaptic links (cholinesterase and receptors kinetics) were apparently not altered in this subpopulation. More probably their slow and often irregular rate of rise arose from some desynchronization of the release process.

9. It is concluded that at the nerve–electroplaque junction evoked transmitter release operates in the form of quanta containing *ca* 10000 acetylcholine molecules; the quanta activate independent but closely adjacent postsynaptic fields. Each quantum is apparently composed of a preferential number of subunits emitted at the same point, or very close to each other. The subunits are delivered synchronously in the majority of events (fast MEPPs) but subunit desynchronization occasionally occurs (slow-rising and composite MEPPs).

INTRODUCTION

The objectives of the present work were to gain information about the arrangement of the quantal release sites in the synaptic space and to address the question of whether the individual quanta might have a substructure. The work was carried out on the electric organ of *Torpedo*, a tissue that is embryologically homologous to the neuromuscular junction. Evoked transmitter release is quantal in the electric organ with one quantum composed of approximately 7–10000 acetylcholine (ACh) molecules (Dunant & Muller, 1986), a value very close to that reported for the motor endplate (Kuffler & Yoshikami, 1975). This raises several interesting questions since the nerve–electroplaque synapse differs from the neuromuscular junction in several cytological aspects. There are no presynaptic specializations similar to the active zones of the endplate (Couteaux & Pécot–Dechavassine, 1973) in the *Torpedo* electric organ, and the synaptic vesicles are almost twice the size of those of the motor nerve terminals.

Normally, the majority of spontaneous events recorded at the endplate are miniature potentials whose amplitude and time course are identical to those of the quantal component of evoked endplate potentials (see Katz, 1969). A certain proportion of 'anomalous' events have nevertheless been regularly noticed in various species. These are potentials (or the related currents) of a much smaller size, or

potentials with a slow and sometimes irregular time course (Kriebel & Gross, 1974; Thesleff & Molgó, 1983; Vautrin & Kriebel, 1991). It has been proposed that spontaneous and evoked quanta are built up of a discrete number of subunits but this is still a matter of controversy (see Matteson, Kriebel & Llados, 1981; Erxleben & Kriebel, 1988*b*). Events of small amplitude have also been recorded in the *Torpedo* electric organ (Muller & Dunant, 1987). These, as well as slow spontaneous potentials, were analysed more quantitatively in the present study with the aim of establishing their relationships with the quantal events and to investigate thereby the space and the time characteristics of transmitter release.

In the present study we also compared our recorded data with the predictions of a theoretical model of synaptic transmission. Our approach was based on previous models (Wathey, Nass & Lester, 1979; Land, Salpeter & Salpeter, 1981; Land, Harris, Salpeter & Salpeter, 1984; Madsen, Edeson & Milne, 1987; Nigmatullin, Snetkov, Nikol'skii & Magazanik, 1988; Bartol, Land, Salpeter & Salpeter, 1991). However, it became necessary to introduce additional features in order to simulate responses to the release of several packets containing various amounts of ACh molecules. We modelled the delivery of packets to either the same spot or to different sites, either synchronously or with different time patterns. Although semi-quantitative, this model made it possible to determine the time and space characteristics of both spontaneous and evoked release of ACh quanta.

METHODS

Fish and chemicals

The fish *Torpedo marmorata*, males and females of various sizes, were obtained from the Station de Biologie marine, Arcachon, France. Slices of electric organ were excised from the anaesthetized fish immersed in tricaine methane sulphonate, 1 g (3 l sea water)$^{-1}$. The tissue was kept in an elasmobranch saline medium of the following composition (mM): NaCl, 280; KCl, 7; $CaCl_2$, 3·4; $MgCl_2$, 1·3; $NaHCO_3$, 5; Hepes buffer, 20; urea, 300; glucose, 5·5. The medium was gassed with 95% O_2 and 5% CO_2 before the experiment; its pH was adjusted between 7·1 and 7·3. The experiments were carried out at room temperature (18–22 °C).

Recording of spontaneous and evoked postsynaptic responses

Electroplaques in the *Torpedo* electric organ are giant flat cells innervated by millions of nerve endings. They are nevertheless very thin and their uninnervated membrane has many micro-invaginations. The input resistance is therefore extremely low in an electroplaque. Another peculiarity of *Torpedo* electroplaques is the absence of voltage dependent channels. The electroplaques are not electrically excitable and their current–voltage relationship is linear (see Bennett, Wurzel & Grundfest, 1961). The low input resistance and the dense innervation makes it practically impossible to record individual miniature potentials with an electrode located in the cytoplasm of a *Torpedo* electrocyte. To obtain reliable recordings, we used another approach (Dunant & Muller, 1986; Muller & Dunant, 1987), in which a limited area of synaptic surface was insulated under a 'loose patch' external electrode. The same type of electrode was used throughout the present investigation. It consisted of fire-polished borosilicate glass pipettes with an internal tip diameter of 5–15 μm. Their resistance was typically 0·3 MΩ in the bath, which increased to about 1 MΩ following positioning against the innervated face of an electroplaque and application of a slight suction (Fig. 1*A*).

Connected to a voltage-clamp device, the loose patch electrode was used both to stimulate the nerve terminals in the area under observation and to record the evoked postsynaptic currents. A brief pulse of depolarizing current was injected in the electrode by shifting the holding potential from ground level to a negative value inside the pipette. Such a stimulation was expected to activate the nerve terminals situated in the patch area, either via opening of voltage-dependent sodium channels (all-or-none response), or by direct opening of voltage-dependent calcium channels (graded response, see Dunant & Muller, 1986). Only the graded response was elicited in

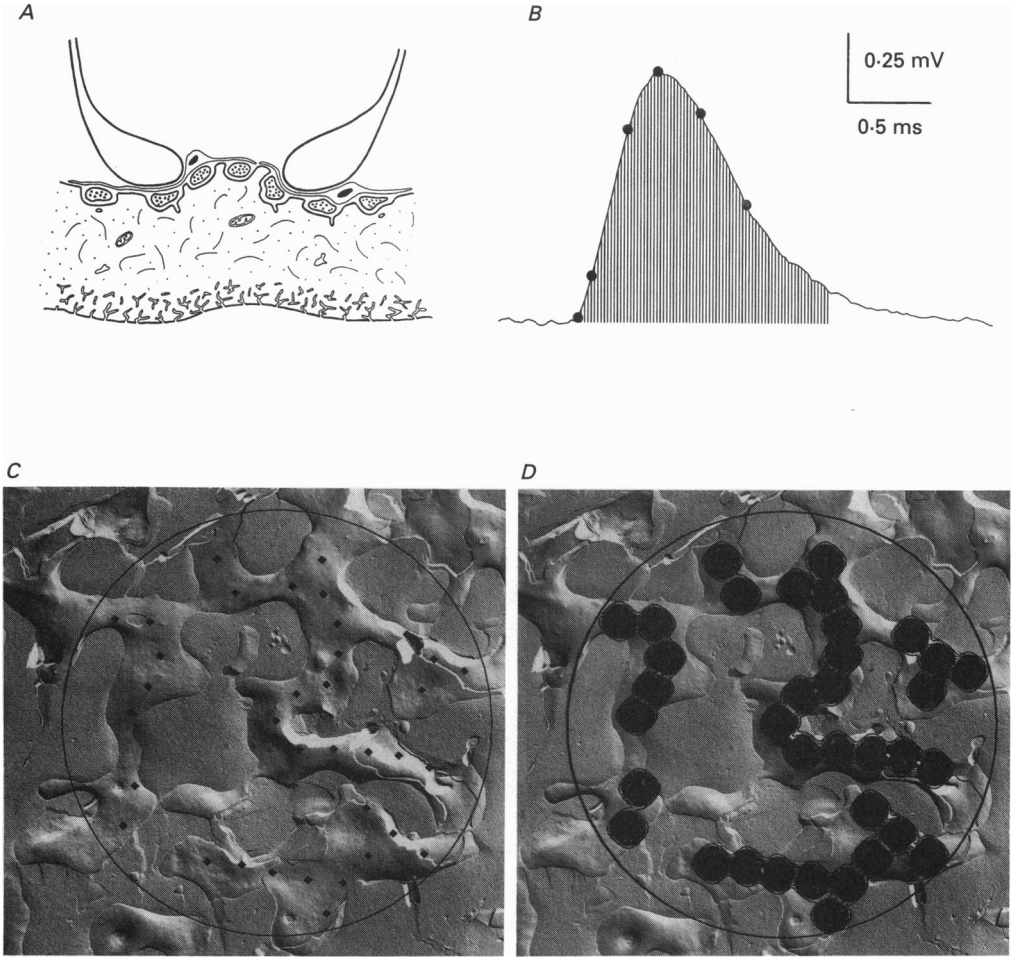

Fig. 1. *A*, schematic drawing showing the presumed position of the external loose patch electrode on a transverse section of a *Torpedo* electroplaque. A slight suction increased the resistance between the interior of the electrode and the bath, allowing it to insulate electrically the patch area under observation. Inner diameter of the electrode 5–15 μm. *B*, external MEPP recorded with an electrode as described in *A*. The points on the trace show: the origin, 20 and 80% of the peak amplitude in the rising phase, the peak, 75% and half-decay from the peak. The parameters determined for each MEPP were: *Amplitude*; *time to peak*, between the origin and the peak; *rise time*, between 20 and 80% of amplitude; *half-decay time*, between maximum and half-amplitude; *surface*, shown as the hatched area integrated between origin, and peak maximum plus twice the half-decay time; *time constant of decay*, between 75% down to 10% of the peak. *C* and *D*, simulation of evoked quantal release in a patch area. The circle illustrates the inner diameter of the electrode (10 μm) superimposed on a freeze fracture replica of the terminal network innervating an electroplaque (electron micrograph from L. M. Garcia–Segura). In *C*, the putative sites of quantal release were disposed on the terminal network at 800 nm from each other. The simultaneous release of one quantum by each release site was then simulated. The ACh concentration computed for the time $t = 0{\cdot}36$ ms (corresponding to the peak of the simulated response) is illustrated in *D*. The quanta appear to spread on adjacent fields, making optimal use of the innervated space.

the present work since we used tetrodotoxin (10^{-6} M, from Calbiochem Co., La Jolla, CA, USA) to block sodium channels. Immediately after the depolarizing pulse, the intrapipette potential was switched back to ground and held at this level to record the currents occurring in the patch under observation. The residual artifact arising in the electrode after the pulse was compensated for by adjusting exponential wave forms to the recorded trace after the head stage of the amplifier. The genuine postsynaptic response picked up by the external electrode was a negative signal. With the voltage-clamp system it was measured as a positive current, represented here. As this current was homologous to the endplate current, the evoked response has been abbreviated to EPC (for electroplaque current).

Spontaneous miniature electroplaque currents (MEPCs) could also be recorded with this device. Significant amounts of noise in the voltage-clamp system, however, made it difficult to analyse properly the time course of MEPCs and to detect events of small amplitude. It was more convenient simply to record them by the potential changes driven by these currents in the external pipette. With this technique, it is possible to obtain records with a very high signal-to-noise ratio (typically 1:50 to 1:100 for a quantum size signal). From previous work on the neuromuscular junction it is known that the waveform of the potential change recorded by an external electrode reflects the time course of the postsynaptic current (Gage & McBurney, 1975). To check this, we recorded spontaneous activity at the same site of a nerve–electroplaque junction, first as MEPPs and then as MEPCs without changing the location of electrodes. The mean time to peak was $0{\cdot}71 \pm 0{\cdot}15$ ms for MEPPs and $0{\cdot}71 \pm 0{\cdot}20$ ms for MEPCs in this particular experiment. The half-decay time was $0{\cdot}72 \pm 0{\cdot}12$ ms for MEPPs and $0{\cdot}84 \pm 0{\cdot}23$ ms for MEPCs (means $\pm$ S.D.). Spontaneous potentials recorded in this way were abbreviated to MEPPs (miniature electroplaque potentials). They were negative signals but they were represented with the converse sign to allow comparison with the above described currents.

Data collection and analysis

Experiments were recorded on VHS tapes using a digital recording system (model VR-10, Instrutech Corp., Mineola, NY, USA). The data were then digitized at high frequency (50 kHz). For spontaneous activity, the peak of external MEPPs, rather than their origin, was detected to trigger the onset of digitization. This was achieved by using a hardware device sensitive to the abrupt change of slope at the top of a peak. All peaks whose amplitude relative to the noise level exceeded an adjustable floating threshold were digitized as 150 points preceding and 60 points following the trigger. The large number of pre-trigger points was needed for full digitization of those MEPPs displaying a very slow rising rate. The advantage of detecting the peak rather than the onset of the signals was to yield optimal discrimination of the smallest events over the noise level and to ensure that MEPPs with a slow rising phase were not missed because of their atypical initial slope. For evoked currents, digitization was triggered by the stimulation artifact.

All digitized traces were stored on hard disk for further analysis. A program was used to determine the origin of the signals and to calculate: amplitude, time to peak, half-decay time, time constant of decay and surface (see Fig. 1*B*). For comparison with reports on muscle spontaneous events, the rise time, between 20 and 80% of the peak amplitude was also calculated in some experiments. The time constant of decay was determined from the least-squares fit of a straight line to a semilogarithmic transform of the decay phase between 75 and 10% of the peak amplitude. The correlation coefficient for the exponential fit was greater than 0·95 in 93 ± 2% of the external MEPPs ($n = 6$ preparations; S.E.M.). When current traces, but not potential traces, were analysed or illustrated, these were digitally filtered with a numerical low-pass 4 kHz filter after acquisition. We checked that such filtering removed the high frequency noise without distorting the waveforms of the currents.

It was found that the nerve–electroplaque junction of *Torpedo* generated a certain proportion of slow-rising and/or slow-decaying MEPPs. We had to find criteria to determine whether a given signal should be considered as a slow- or as a fast-MEPP. A difficulty arose from the fact that in the electric organ the half-decay time and time to peak were both correlated with the amplitude of the signals (see Fig. 4). The larger events had a longer rising and a longer decaying phase. Thus, selecting all MEPPs whose time to peak or half-decay time exceeded a fixed limit would bias the discrimination (some large events would be wrongly taken as slow-MEPPs). We overcame this difficulty using the following procedure: the regression line of the plot of time course parameters *vs.* amplitude was computed and 'normalized' values were calculated for amplitude, time to peak and half-decay time from their position relative to the regression line. A Gaussian curve was fitted on the left part of the normalized distribution relative to the mean. Slow-rising (or slow-decaying)

MEPPs were selected as those events whose 'normalized' time-to-peak (or 'normalized' half-decay time) was longer than the mean plus twice the standard deviation of the normalized parameter of the whole population.

In addition we paid attention to the rising slope of signals, either by computing the overall slope between 10 and 90% of the peak, or by determining the change of slope occurring in a certain percentage of external MEPPs. To do this, individual digitized signals were displayed on the computer screen; a program was developed for manual fitting of two straight lines on the rising phase of the MEPP, one on the segment preceding and the other one on the segment following the change in rising rate (see Fig. 6*B*).

Theoretical model of nerve–electroplaque transmission

Our aim was to understand to what extent the shape of normal or abnormal postsynaptic currents could bring information about the space and time characteristics of transmitter release. For this purpose we designed a bidimensional model of synaptic transmission in which the release of several packets of transmitter could be simulated with a variety of space and time patterns. Our model can be thus considered as an extension of previous simulations, most of them were used for describing the response to a single quantum (Wathey *et al.* 1979; Land *et al.* 1981, 1984; Madsen *et al.* 1987; Nigmatullin *et al.* 1988). The calculations were based on parameters described for *Torpedo* when available and were performed by solving numerically simultaneous partial differential equations for ACh diffusion, hydrolysis by acetylcholinesterase (AChE), binding to and unbinding from ACh receptors, and conformational change of the channel from the closed to the open state. The distribution of free ACh molecules and the various states of the receptor were characterized by density functions of space and time. The total number of ACh receptors (AChR) with the channel in the conducting conformation at time t was compared to the waveform of the recorded signals.

Dimensions of the synaptic space and kinetics of ACh release. The synaptic space was represented as a disk of radius R_{post} (taken as 0·75 μm, see later) and height equal to the height of the synaptic cleft H_c (50 nm). When ACh reached the edge of the cleft, it was removed from the simulation. As in most previous models, the vertical co-ordinate was omitted by assuming instantaneous diffusion of ACh and even distribution of both AChR and AChE across the length of the cleft. The cleft height determined the constant of proportionality between the surface densities and the volume densities. Making allowance for the vertical diffusion did not significantly change the behaviour of the model. Moreover, in the three-dimensional Monte Carlo simulation of Bartol *et al.* (1991), the time required for even distribution of ACh across the cleft in front of the release point was found to be very short, in the range of a few microseconds. We represented the synaptic cleft as a bidimensional plane sheet divided in small squares of length Δx (25–100 nm) and of height H_c, in which ACh simultaneously diffused, was hydrolysed and interacted with receptors. Explicit finite difference methods were used to extrapolate a new set of densities from one time step to the next.

The quantal size Q was taken as 10000 ACh molecules (Dunant & Muller, 1980). While ACh release was assumed to be instantaneous in previous simulations, our model was designed to deliver synchronous or asynchronous packets of ACh, either from the same spot or from release sites separated from each other by various distances. At the beginning of the injection, the rate of release was maximal; then it decreased linearly and subsided after 150 μs. Such progressive release caused only little alteration to the shape and the size of the response. With instantaneous release, a peak of 1758 open receptor channels was reached after 0·30 ms; with the progressive release, these values were 1719 channels and 0·35 ms. The progressive release allowed more accurate calculations since the steep density gradient occurring at time $t = 0$ with instantaneous release was avoided.

Equations of the model and parameters of simulation. The fate of ACh molecules after injection in the cleft was assumed to be determined by three processes, as follows.

(i) *Diffusion*, away from the point of release, described by the following bidimensional equation:

$$\frac{\delta u_1}{\delta t} = D\left[\frac{\delta^2 u_1}{\delta x^2} + \frac{\delta^2 u_1}{\delta y^2}\right],$$

where D was the ACh diffusion coefficient. We adopted the value of 10^{-10} m^2 s^{-1} for this parameter (see previous models); u_1 was the ACh concentration at the spatial co-ordinate (x, y) and at the time t. Loss was modelled by removing from the simulation any free ACh that reaches the circular limit of the cleft of radius R_{post}.

(ii) *Interaction with postsynaptic receptors.* We adopted the standard kinetics of two-stage sequential binding and channel opening (Adams, 1981) described by

$$2A + Rc \underset{K_{-1}}{\overset{2K_1}{\Leftrightarrow}} A + ARc \underset{2K_{-2}}{\overset{K_2}{\Leftrightarrow}} A_2Rc \underset{\alpha}{\overset{\beta}{\Leftrightarrow}} A_2Rc^*,$$

where A was an ACh molecule; Rc was a receptor molecule containing 2 ACh binding sites; ARc was a singly bound receptor; A_2Rc was a doubly bound receptor in the closed state; A_2Rc^* was a doubly bound receptor in the open state; K_1 and K_2 were the forward binding constants, K_{-1} and

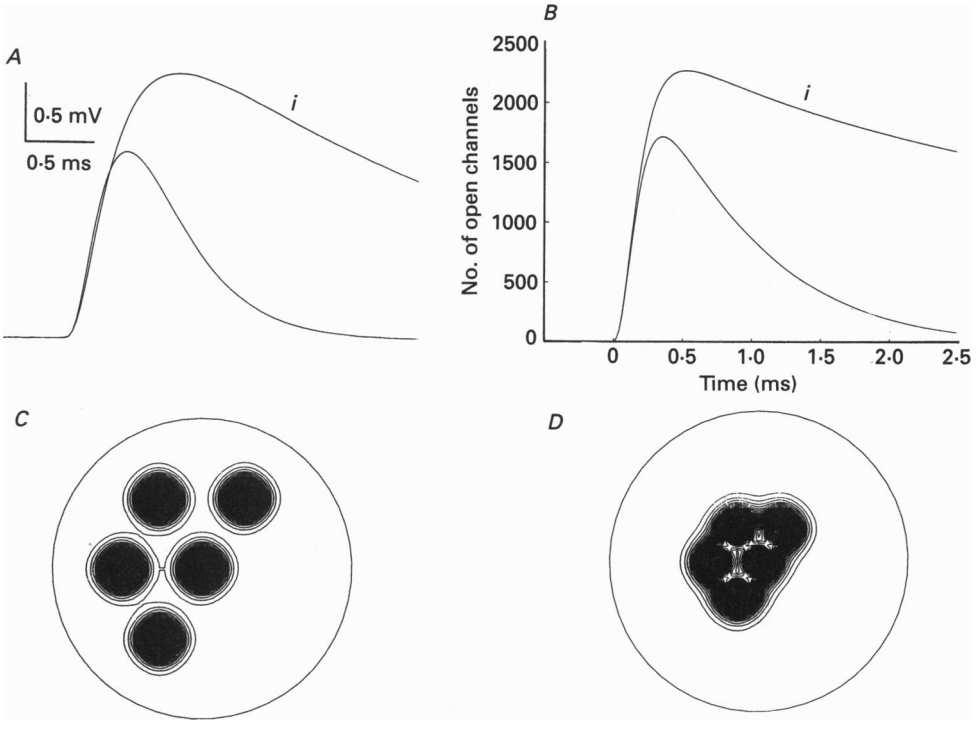

Fig. 2. Comparison of MEPPs recorded in the electric organ (*A*) with simulated responses (*B*). External MEPPs were recorded with a loose patch electrode with cholinesterase activity either intact or inhibited by 50 μM phospholine (*i*). Each trace is the average of 208 individual MEPPs. The simulated responses were obtained by delivering 10000 ACh molecules on a single site of the synaptic space. The curve with AChE active had an amplitude of 1719 open receptor channels. With AChE taken as inactive, the amplitude was 2265 open channels. *C* and *D*, bidimensional simulation of ACh concentration profiles resulting from injection of 5 ACh packets composed of 1000 molecules each. In *C*, the distances separating the 5 release sites were 600 nm; in *D*, 300 nm. The concentrations are displayed as contour levels, one line corresponding to a concentration of 1 μM; outside of these contours, the concentrations were less than 5% of their maximal value in each picture. The time corresponds to the peak of the relevant simulated signal (0·22 ms in *C* and 0·24 ms in *D*). The circular limits show postsynaptic surfaces of 1·14 μm radius. Overlapping of fields acted on by the individual packets could be visualized for 300 nm, but not for 600 nm.

K_{-2} were the unbinding rate constants; β and α were the channel conformation rate constants. No co-operativity was assumed between either binding step or unbinding step (see Land *et al.* 1981, 1984; Bartol *et al.* 1990), so that $K_1 = K_2 = K_+$ and $K_{-1} = K_{-2} = K_-$. Quantitative values of the parameters were taken from work on *Torpedo* electric organ if available, otherwise from work on

neuromuscular junction. They were $K_+ = 5\ 10^7$ l mol^{-1} s^{-1}; $K_- = 10^4$ s^{-1}; $\beta = 20000$ s^{-1} (Colquhoun & Sackmann, 1985; Colquhoun & Ogden, 1988). In the present simulation, we adopted $\alpha = 5000$ s^{-1} for the mean rate of channel closing. This was higher than typical values of the endplate (500–2500 s^{-1}; Colquhoun & Ogden, 1988). Indeed single channel recordings indicated that the mean open time of the channel was relatively short in the electric organ (0·6 ms), while at both synapses the receptors exhibited similar binding/unbinding and opening characteristics (Sakmann, Methfessel, Mishina, Takahashi & Takai, 1985). Consistent with these data, we found that the rate of MEPP decline in the electric organ was significantly faster than that usually reported for the endplate quantal event. As for the density of receptor in the subsynaptic membrane, like in the muscle, values of 10000 receptors or 20000 binding sites per μm^2 were reported in the *Torpedo* electric organ (Heuser & Salpeter, 1979).

(iii) *Hydrolysis by AChE.* This was described in the following simplified form (see Wathey *et al.* 1979)

$$A + E + H_2O \xrightarrow{K_{e1}} AE \xrightarrow{K_{e3}} E + \text{acetate} + \text{choline} + H^+,$$

where E is the free catalytic site of AChE; AE was the complex enzyme–ACh; K_{e1} was the velocity constant of binding between ACh and AChE; K_{e3} was the rate constant of hydrolysis. The values used in the model were $K_{e1} = 2 \times 10^8$ s^{-1} and $K_{e3} = 16000$ s^{-1} (Rosenberry, 1975). Since we were not aware of any direct measurement of the density of AChE sites in the *Torpedo* electric organ, we adopted the endplate value of 2600 (Salpeter, Rogers, Kasprzak & McHenry, 1978).

Validation of the model. With this set of parameters, emission of one quantum gave rise to a simulated response whose amplitude at the peak corresponded to 1719 open receptor channels; a value that was in the range of the estimations made at the motor endplate (Anderson & Stevens, 1973) and at the *Torpedo* nerve–electroplaque junction (Dunant & Muller, 1986). The time to peak of the simulated MEPP was 0·3 ms, its half-decay time was 0·64 ms. The results of simulations obtained with active or inactive AChE are shown in Fig. 2*B* where the responses are expressed as number of ACh receptor channels in the open configuration as a function of time t. These simulated responses are to be compared with the experimental averaged MEPPs recorded in the electric organ under control conditions and after cholinesterase inhibition (Fig. 2*A*). To inhibit cholinesterase in this experiment we used phospholine (ecothiopate iodide, 10^{-5} M for 30 min, a generous gift from Ayerst Laboratories, New York, USA). In all other experiments cholinesterase was not inhibited.

The area of the functional synapse was an important parameter since it determined the amount of ACh lost out of the cleft by diffusion. We adjusted this parameter as follows: when AChE is inhibited, ACh molecules can bind and activate the receptors several times before diffusing out of the cleft; the falling phase of MEPPs is consequently lengthened and the rate of decay depends upon the interplay between binding to receptors and diffusion, and upon the size of the cleft, a process called 'buffered diffusion' by Katz & Miledi (1973). In the electric organ, we found that upon inhibition of AChE by phospholine, MEPP half-decay time was lengthened by a factor of 4·6 (Fig. 2*A*). In the model, the same prolongation of the falling phase with AChE inactive was obtained with a postsynaptic surface of radius $R_{post} = 0{\cdot}75$ μm; this value compared well with the average size of contacts between nerve terminals and electroplaque membrane measured in morphological preparation (0·5–2·0 μm; Heuser & Salpeter, 1979; Dunant & Muller, 1986). In addition, AChE inhibition caused the amplitude of physiological MEPPs to be increased by a factor of 1·4 and the time-to-peak to be prolonged by 1·9 (Fig. 2*A*). Similar changes were obtained from four different experiments (range of amplitude increase: 1·2–1·7; see also Dunant & Muller, 1986). When AChE was taken as inactive in the model, the simulated MEPP also displayed increased amplitude and time to peak (Fig. 2*B*). Although the model parameters were not known with a great precision, it simulated the generation of quantal events in a satisfying, although semi-quantitative, manner. It could therefore provide useful comparison with the physiological signals.

RESULTS

Time and space characteristics of evoked quantal release

Two types of calcium-dependent electroplaque currents (EPCs) can be evoked by local depolarization of nerve endings in a patch area of nerve–electroplaque junction. The 'all-or-none' response is obtained at a relatively low threshold of stimulation

and is tetrodotoxin sensitive. It is expected to result from the generation of a Na^+-dependent presynaptic action potential. The other type of response is the 'graded response', whose amplitude increases with stimulations of increasing intensity, and which is tetrodotoxin resistant. The graded response is thought to result from direct activation of presynaptic Ca^{2+} channels by the depolarizing pulses (Dunant & Muller, 1986).

We were interested in the time characteristics of homogeneous sets of graded EPCs of different sizes. In the majority of experiments, graded EPCs elicited in this way exhibited a rapid and homogeneous time course. In some experiments, however, EPCs had an irregular shape with a succession of steps suggesting desynchronization of quantal release. Such desynchronized EPCs were not included in the present description. The preparation was treated with tetrodotoxin (10^{-6} M) to block the all-or-none response. The intensity of electrical pulses delivered at 0·5 Hz through the electrode was first adjusted to evoke the release of a few quanta. These could be readily distinguished when successive EPCs were superimposed on their origin (Fig. 3*A*). Then, while continuously recording, the strength of the stimulation was increased until EPCs of maximal amplitude were obtained. In this experiment, the response to a single quantum had an amplitude of $1{\cdot}8 \pm 0{\cdot}4$ nA (mean $\pm$ S.D. from a Gaussian curve fitted on the first quantal peak of the amplitude histogram; not illustrated), and the quantal content of the maximal EPC was eleven, which means that a maximum of eleven quanta could be produced in the patch area under observation.

The plot of the time to peak *vs.* amplitude is shown for this family of EPCs in Fig. 3*B*. For the smallest events, whose size was in the range of the response to one or two quanta, the time to peak seemed to increase with increasing amplitude. This probably reflected the relationship observed with monoquantal events of a different size (see later). With quantal contents larger than two, however, there was no significant relationship between time to peak and amplitude. All responses had approximately the same time to peak, whatever their amplitude. In contrast, when the decline of EPCs was analysed, a positive relationship was seen between the amplitude and the half-decay time, for amplitudes between two and eleven quanta (Fig. 3*C*). Thus, the quantal responses of this family exhibited simple additivity during their rising phase. On the other hand, the positive relationship found between amplitude and half-decay time suggested that the quanta no longer acted independently during the late phase of the EPC, but might activate overlapping postsynaptic areas (see Hartzell, Kuffler & Yoshikami, 1975).

To test this hypothesis, we tried to estimate the distance separating the quantal release sites in the electric organ by using the theoretical model described above. We simulated the effects of ten packets of 10000 ACh molecules each delivered synchronously at time $t = 0$ on spots situated at various distances from each other. As described in previous simulations (Land *et al.* 1981, 1984; Bartol *et al.* 1991), ACh is expected to diffuse around the release spot and activate a disc of postsynaptic receptors whose size enlarges as a function of time. Cholinesterase activity, among other factors, will limit the diameter of the disc. Figure 3*D–F* shows the predictions of the model when the gap separating the release spots was reduced from 1000 to 0 nm. When the packets were delivered at large space intervals, the fields were fully

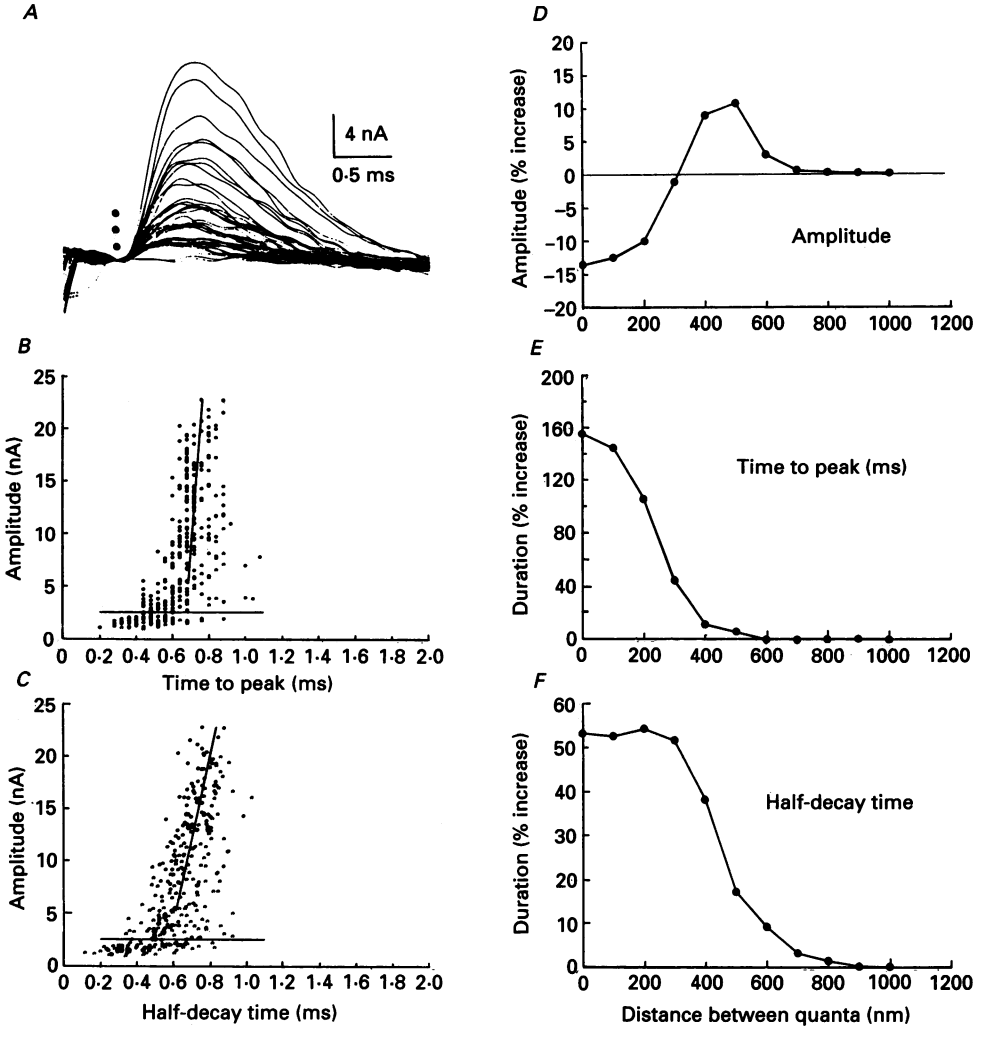

Fig. 3. *A–C*, time characteristics of evoked EPCs recorded from a patch area of electric organ. *A* shows a series of 40 graded EPCs evoked by local depolarization of nerve endings. They were superimposed on their origin. Black dots show EPC amplitudes corresponding to 1, 2 or 3 quanta. *B*, plot of amplitude *vs.* time to peak of 322 EPCs. *C*, plot of their amplitude *vs.* half-decay time. In *B* and *C*, the horizontal line shows twice the standard deviation above the mean amplitude of monoquantal responses (unitary EPCs). Regression lines were calculated for EPCs corresponding to 3 quanta or more. *D–F*, simulation of evoked multiquantal release of ACh: dependence of the amplitude (*D*), of the time to peak (*E*), and of the half-decay time (*F*) of a response to 10 quanta upon the distance separating the release sites. Note the different ordinate scale in each graph. The data were expressed as changes from the value expected from addition of 10 times the unitary response (level 0).

independent and the composite response during the whole time course was the exact addition of individual responses. For smaller gaps, the relationship between the amplitude of the simulated EPCs and the space intervals between quanta was complex (Fig. 3*D*). For distances larger than 700 nm, the size of the composed

response was as expected from simple additivity of the unitary responses. A relative potentiation of amplitude was seen with distances ranging from 300 to 700 nm. With release sites less than 300 nm apart, the interaction of ten quanta on the same field resulted in a reduction of the composite response with respect to the size expected from a simple addition. The distance separating the ten quantal release sites from each other also affected the time to peak (Fig. 3*E*), and the half-decay time (Fig. 3*F*). The time to peak was prolonged when quanta were delivered from spots less than 600 nm apart, while lengthening of the decay phase was detectable with spots less than 900 nm apart.

Thus, the positive correlation between the amplitude and the half-decay time observed with the EPCs actually recorded at the nerve–electroplaque junction (Fig. 3*A* and *C*). It was suggested, by comparison with the model (Fig. 3*F*), that the quanta *in situ* were released from sites less than 1000 nm apart. With distances shorter than 600 nm the time to peak would also be correlated with amplitude, but it was not (Fig. 3*B* and *E*). It seems therefore reasonable to estimate that the intervals separating the quantal release sites from each other ranged within a window of 600–1000 nm in the electric organ.

To help visualization of this spatial organization, the above simulation was related to the anatomical structure of a *Torpedo* electroplaque (Fig. 1*C* and *D*). In the left picture, quantal release sites separated from each other by 800 nm were disposed on an electron micrograph of the innervated membrane. The simultaneous release of one quantum by each site was then simulated and the changes in ACh concentration were followed as a function of time. The right picture shows ACh distribution after 0·36 ms of simulation, that is, at a time corresponding to the peak of the computed response.

External MEPPs with homogeneous and rapid time characteristics

The same loose patch electrodes were used to record the potential changes generated by the action of spontaneously released ACh packets. Before starting any analysis, we decided to collect on several preparations a large number of spontaneous events, without rejecting any because of its abnormal size or time course.

The majority of external MEPPs exhibited homogeneous and rapid time characteristics. These were called fast-MEPPs and they will be described first. Fast-MEPPs were selected in two steps, as illustrated in Fig. 4, for an experiment in which 2572 MEPPs were recorded from a single patch. The scatter diagram of Fig. 4*A* shows their half-decay time *vs.* amplitude relationship. It was characterized by a dense cloud corresponding to a relatively homogeneous MEPP population which exhibited a positive relationship between amplitude and half-decay time. Particular MEPPs situated to the right side of the cloud displayed an abnormally long decline. First, these slow-decaying MEPPs were selected under visual inspection as those signals which had a clearly prolonged or irregular falling phase when compared to a representative sample of superimposed fast-MEPPs. Second, by using the statistical procedure described in the Methods we defined for each amplitude a maximal acceptable value for the half-decay time, determining a limit which is illustrated as a straight line in Fig. 4*A*. In this experiment, 268 points, that is, 10·4 % of all MEPPs were localized to the right of this line and were thereby identified as slow-decaying events. Their half-decay time distribution is shown in Fig. 4*B* in black superimposed

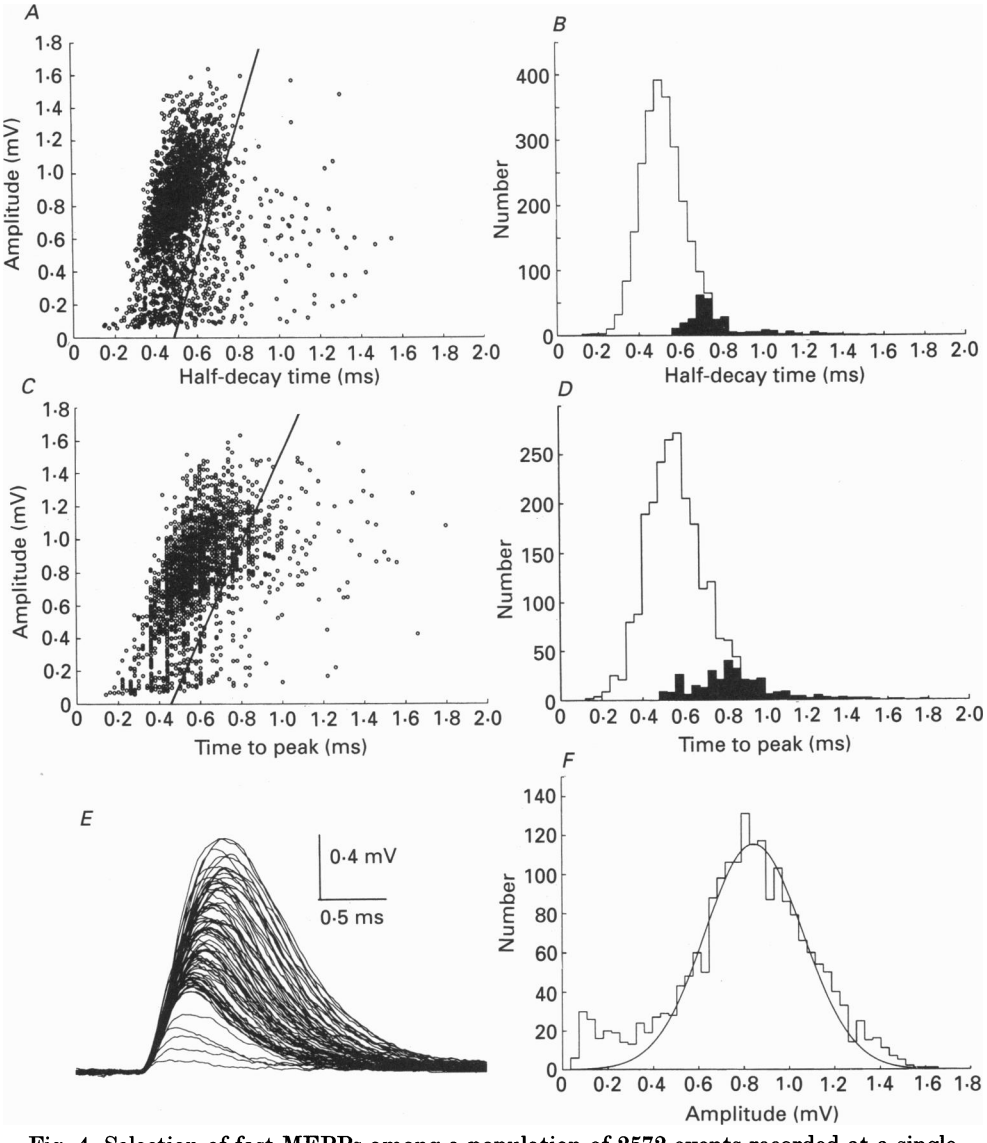

Fig. 4. Selection of fast-MEPPs among a population of 2572 events recorded at a single patch. The mean frequency was 9·2 Hz. *A*, plot of amplitude *vs.* half-decay time for the whole population; fast-decaying and slow-decaying MEPPs are respectively localized to the left and to the right of the straight line. *B*, half-decay time distribution of all MEPPs; the distribution of the 268 MEPPs characterized by a slow rate of decay is superimposed in black. *C*, plot of amplitude *vs.* time-to-peak of the remaining 2304 MEPPs, retained for their fast rate of decay. In this population, fast-rising MEPPs are to the left and slow-rising MEPPs are to the right of the limit line. *D*, time-to-peak distribution of fast-decaying MEPPs; the distribution of the 315 events which were selected for their slow-rising phase is shown in the filled histograms. The remaining 1989 MEPPs had both a rapid rise and a rapid decay; a sample of these fast-MEPPs is shown in *E*. The amplitude distribution of fast-MEPPs is illustrated in *F*; the Gaussian curve was fitted on the right flank of the distribution of the main population (quantal-MEPPs). Events smaller than the mean amplitude of this mode minus twice the standard deviation were considered as sub-MEPPs.

on the distribution of the whole population. Both approaches gave similar results. For six preparations from different fishes the incidence of slow-decaying MEPPs was found to be $14{\cdot}2 \pm 3{\cdot}0\%$ (S.E.M.).

Slow-rising MEPPs were identified in a similar way, either by visual inspection of data or on the plot of time to peak *vs.* amplitude, from the population previously

TABLE 1. Comparison between the characteristics of fast-MEPPs and of slow-rising MEPPs

	Fast-MEPPs	Slow-rising MEPPs	P	n
Amplitude (mV)	$1{\cdot}25 \pm 0{\cdot}24$	$1{\cdot}08 \pm 0{\cdot}19$	$< 0{\cdot}025$	12
Time to peak (ms)	$0{\cdot}43 \pm 0{\cdot}02$	$0{\cdot}62 \pm 0{\cdot}04$	$< 0{\cdot}001$	12
Half-decay time (ms)	$0{\cdot}45 \pm 0{\cdot}02$	$0{\cdot}48 \pm 0{\cdot}02$	n.s.	12
Constant of decay (ms)	$0{\cdot}35 \pm 0{\cdot}01$	$0{\cdot}36 \pm 0{\cdot}01$	n.s.	6
Surface (mV ms)	$0{\cdot}62 \pm 0{\cdot}08$	$0{\cdot}72 \pm 0{\cdot}09$	n.s.	7

Results are means $\pm$ S.E.M. of results obtained in n preparations from different fish. The statistics relate to analysis of the differences between paired mean values from each experiment, using Student's paired t test. n.s.: no significant difference.

selected for a rapid decay (Fig. 4*C*). Again, the scatter diagram indicated a main population with a positive time to peak *vs.* amplitude relationship, whereas slow-rising MEPPs could be recognized on the right of the dense cloud, Figure 3*D* shows the time-to-peak distribution of the MEPPs, with the slow-rising ones illustrated in black. In this particular experiment, the incidence of slow-rising MEPPs was 12·5% of all recorded signals. A mean value of $11{\cdot}1 \pm 1{\cdot}2\%$ was obtained from experiments carried out on six fishes.

Once the two groups of slow MEPPs were removed and reserved for separate analysis, the initial host of 2572 MEPPs in the experiment of Fig. 4 was reduced by 77% to 1989 MEPPs. The remaining population was composed of fast-MEPPs characterized by homogeneous rising and declining rates; a few examples are shown in Fig. 4*E*. Several populations of fast-MEPPs were obtained similarly from six separate experiments and pooled for the following description. Fast-MEPPs represented on average $74{\cdot}8 \pm 3{\cdot}0\%$ of all recorded events.

Fast-MEPPs displayed positive monotonic relationships both between the amplitude and the half-decay time (Fig. 4*A*), and between the amplitude and the time to peak (Fig. 4*C*). Thus, the larger a signal, the longer its rising phase and the slower its decay (see Fig. 4*E*). The mean characteristics of MEPPs recorded from six to twelve preparations are given in Table 1. The mean rise time was $0{\cdot}19 \pm 0{\cdot}02$ ms, which corresponded well to the rise time of endplate MEPCs (see Discussion). The decline was relatively rapid in the electric organ. The mean half-decay time was less than 0·50 ms and the mean time constant of decay was $0{\cdot}35 \pm 0{\cdot}01$ ms.

Although the fast-MEPPs had a homogeneous time course, their amplitude distribution was rather broad (Fig. 4*F*). It was bimodal, with a main population distributed in a bell-shaped manner (quantal-MEPPs). In addition, a second class of MEPPs (sub-MEPPs) had a much smaller amplitude and a distribution skewed towards the background noise. The percentage of sub-MEPPs in the population of fast-MEPPs was determined as explained in Fig. 4. It was $10{\cdot}8 \pm 1{\cdot}4\%$ (12 preparations) in the present series of experiments, confirming previous results on this preparation (Muller & Dunant, 1987).

External MEPPs with a slow or irregular time course

Special attention was paid to MEPPs characterized by a slow rate of rise in spite of a rapid decay. These slow-rising MEPPs displayed a great variety of shapes (Fig. 5). Some had a foot-like, slow-starting rise which lasted from a few microseconds up

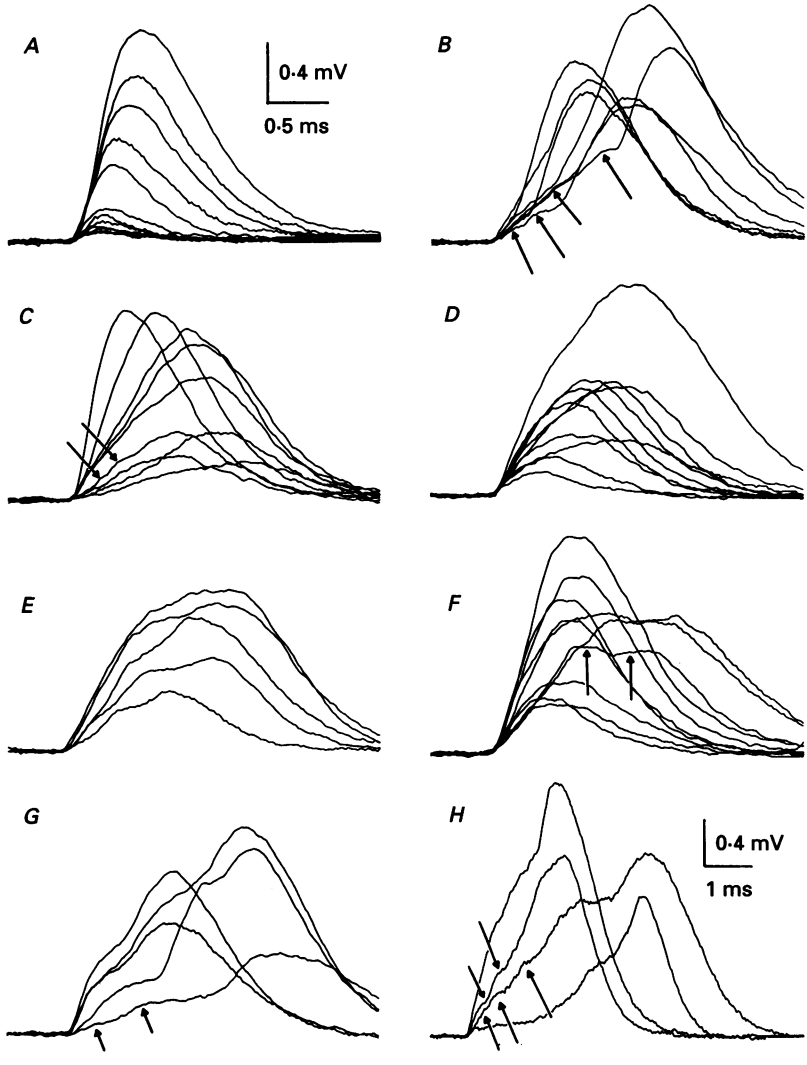

Fig. 5. Types of slow-rising but fast-decaying MEPPs recorded in the electric organ of *Torpedo*. All signals, except those in *H*, were taken from the experiment depicted in Fig. 4. Arrows point to oscillations on the rising phase of some slow signals. *A*, examples of fast-MEPPs. *B*, slow-rising MEPPs with a sudden acceleration of the rising rate ('foot-MEPPs'). *C*, MEPPs with a slow but rather continuous rate of rise. *D*, slow-rising MEPPs with a convex rising phase. *E*, MEPPs with abrupt deceleration of rising rate ('shoulder-MEPPs'). *F*, same as in *E*, but with a plateau-like top; *G*, slow-rising MEPPs with multiple inflexions. *H*, MEPPs displaying the slowest rising phase observed in the whole set of experiments; note the different time scale.

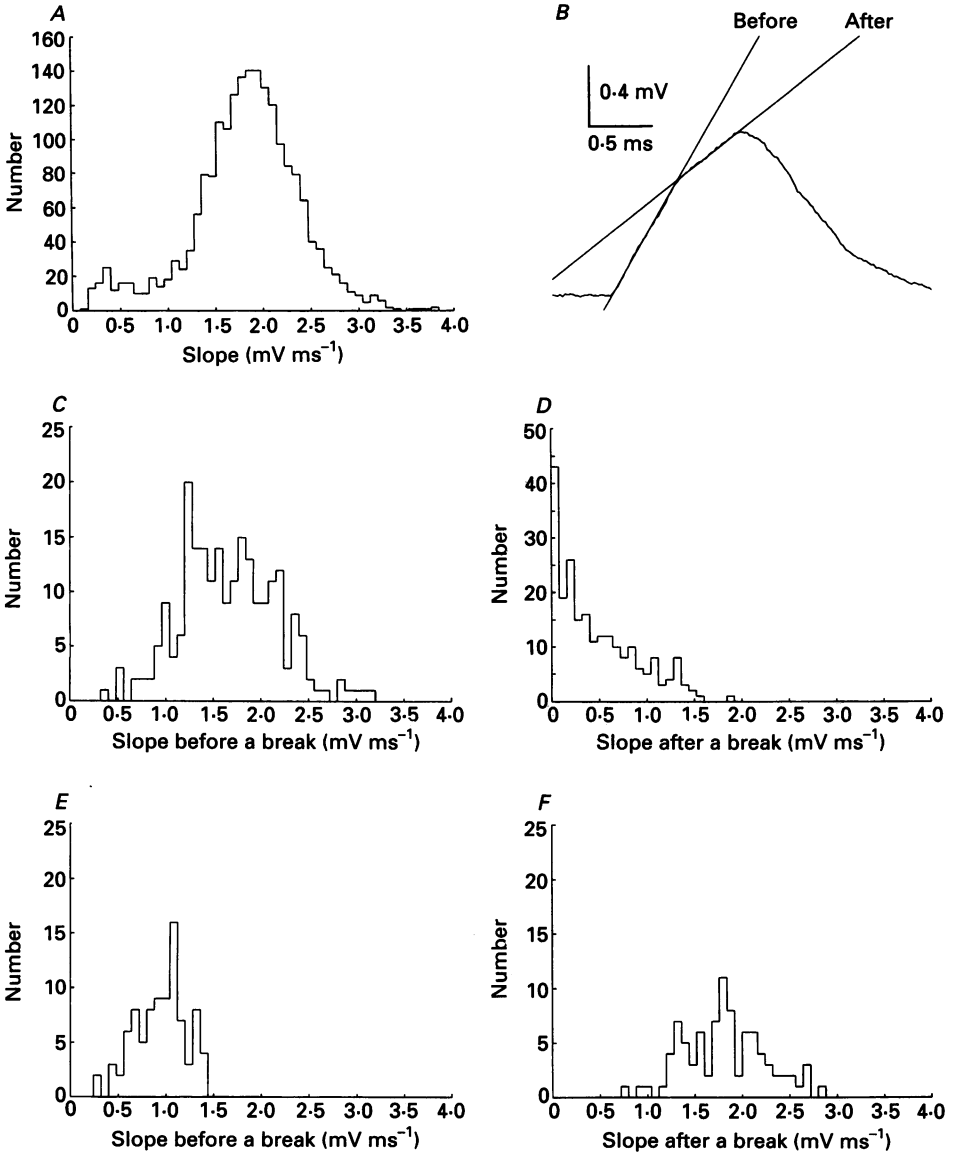

Fig. 6. Histogram analysis of the slopes characterizing fast-MEPPs and slow-rising MEPPs. *A*, slope distribution of 1989 fast-MEPPs previously selected for their rapid time course (see Fig. 4); the mean slope of the whole population was $1{\cdot}83 \pm 0{\cdot}01$ mV ms^{-1}. A Gaussian mode can be seen with a mean at 1·9 mV ms^{-1} and a second mode arising from MEPPs of small amplitude displayed a skewed slope distribution. *B*, procedure by which the slopes before and a break were determined on the rising phase of a shoulder-MEPP. The trace was displayed on the computer screen and a straight line was fitted by eye on each segment of the rising trace. The same procedure was used for 'foot-MEPPs'. *C*, distribution of the initial rising slopes of 223 'shoulder-MEPPs'; the mean was $1{\cdot}67 \pm 0{\cdot}04$ mV ms^{-1}. *D*, distribution of the shoulder-MEPPs rising rate after the deceleration; the mean was $0{\cdot}48 \pm 0{\cdot}03$ mV ms^{-1}. *E*, distribution of the rising slope of 90 'foot-MEPPs' before the acceleration of rise; the mean was $0{\cdot}95 \pm 0{\cdot}03$ mV ms^{-1}; *F*, the same after the acceleration; the mean was $1{\cdot}84 \pm 0{\cdot}05$ mV ms^{-1}.

to 1 ms or more, followed by an acceleration of their rising rate (Fig. 5*B*). Others had a slow but continuous rate of rise, either with a constant slope (Fig. 5*C*), or with a convex appearance (Fig. 5*D*). A break, or shoulder was seen on the rising phase of other MEPPs (Fig. 5*E* and *F*). Some extreme examples of these, with a plateau-like summit of up to about 1 ms duration are shown on Fig. 5*F*. Finally, some events displayed several inflexions on their ascending phase (Fig. 5*G*). Close inspection of the signals actually revealed that the rising phase of many slow-rising MEPPs had a wavy appearance (arrows in Fig. 5), suggesting a composite structure. In the experiment illustrated in Fig. 5*A–G*, maximal time to peak was around 2 ms. In other cases, MEPPs with rising phase up to 5 ms were occasionally observed. Some examples of these are shown in Fig. 5*H* with a different time scale.

Table 1 compares the characteristics of slow-rising MEPPs to those of fast-MEPPs. The time to peak of slow-rising MEPPs was of course longer (this was the criterion for selecting them). An important point should be noticed: the mean amplitude of slow-rising MEPPs was significantly smaller than that of fast-MEPPs. On the other hand, the mean half-decay time, the constant of decay and the surface did not differ significantly in the two populations.

Additional information could be gained by comparing the slope of slow-rising MEPPs to the slope of fast-MEPPs. The distribution of the fast-MEPPs rising slopes (Fig. 6*A*) was similar to the distribution of amplitudes (see Fig. 3*F*); there was a main population with a Gaussian distribution of slopes and a second population characterized by a slower slope. For each individual fast-MEPP the slope was actually related to amplitude, as it could be anticipated from examination of the record traces (not illustrated).

The change of slope occurring on the ascendent phase was investigated for two types of slow-rising MEPPs: those with a foot (Fig. 5*B*) and those with a shoulder (Fig. 5*E* and *F*); they were selected because they had one and only one identifiable point of break. Figure 6*B* illustrates the procedure by which the change of rising slope was computed for a shoulder-MEPP. The distribution of the slopes measured before and after the break of 223 shoulder-MEPPs are shown on Fig. 6*C* and *D*, respectively. Before the break the slopes were close to the distribution obtained with the Gaussian population of fast-MEPPs, but their mean was slightly shifted toward smaller values (compare Fig. 6*C* with Fig. 6*A*). This observation was confirmed with six preparations from different animals in which shoulder-MEPPs were constantly found to start with slopes on average ($2{\cdot}24 \pm 0{\cdot}26$ mV ms^{-1}) smaller than the mean rising rate of fast-MEPPs of the quantal population ($3{\cdot}29 \pm 0{\cdot}82$ mV ms^{-1}); the difference was significant with Student's paired t test ($P < 0{\cdot}05$). From the proportionality between amplitude and slope just mentioned, this means that shoulder-MEPPs had an initial slope that destined them to reach, if the change of rising rate had not occurred, an amplitude slightly smaller than expected for a mean sized fast quantal-MEPP. At the break the slope became smaller: it ranged from zero (MEPPs with plateau-like summit) to *ca* 1·5 mV ms^{-1} (Fig. 6*D*).

The rising slope of the ninety foot-MEPPs showed characteristics that were opposite to those of shoulder-MEPPs. The initial rise of foot-MEPPs was similar to the slope of the sub-MEPP population (compare Fig. 6*E* with Fig. 6*A*). On the other hand, after the acceleration of the rising rate, the slopes of the foot-MEPPs reached values whose distribution was close to that of the quantal population of fast-MEPPs

(Fig. 3*F*). In the whole set of experiments, the rapid portion of foot-MEPPs had a mean slope ($3{\cdot}4 \pm 0{\cdot}96$ mV ms^{-1}) that was not significantly different from the mean rate of rise of quantal fast-MEPPs ($3{\cdot}29 \pm 0{\cdot}82$ mV ms^{-1}).

TABLE 2. Occurrence of slow-rising MEPPs and of sub-MEPPs at different frequencies

Instantaneous frequency (Hz)	Slow-rising MEPPs (%)	Sub-MEPPs (%)
< 20	$10{\cdot}1 \pm 1{\cdot}6$	$11{\cdot}5 \pm 2{\cdot}7$
20–40	$11{\cdot}4 \pm 0{\cdot}7$	$10{\cdot}1 \pm 3{\cdot}0$
> 40	$11{\cdot}2 \pm 1{\cdot}9$	$8{\cdot}9 \pm 1{\cdot}6$

Data were pooled results from three preparations. In each experiment, the MEPPs were classed according to their 'instantaneous frequency' (see text). The values found at the different frequencies did not significantly differ from each other.

Frequency dependence of slow-rising MEPPs and of sub-MEPPs

In a given experiment, the slow-rising MEPPs or the small MEPPs occurred at any time during the recording period. They were intermingled with the dominant population of fast-MEPPs. We were interested in analysing to what extent the frequency had any effect on the occurrence of slow-rising MEPPs and sub-MEPPs. The frequency of MEPPs recorded with an external patch electrode in the *Torpedo* electric organ was rather variable, even on a same site of measurement and within a shorter period of observation. Sometimes long periods of low frequency or even complete silence were interrupted by brief high frequency bursts. The intervals separating a given MEPP from the preceding and from the following events were measured; the two intervals were averaged and an 'instantaneous frequency' was calculated for each MEPP as the inverse of the mean interval. Three sets of MEPPs were defined, corresponding to instantaneous frequencies (i) lower than 20 Hz, (ii) between 20 and 40 Hz, and (iii) higher than 40 Hz. The occurrence of fast-MEPPs, slow-rising MEPPs and sub-MEPPs was counted in the three sets. Table 2 shows pooled data for 14 213 MEPPs recorded in three experiments (including that of Fig. 5) in which the frequency showed conspicuous variations. It can be seen that occurrence of either the sub-MEPPs and slow-rising MEPPs does not depend on the instantaneous frequency.

Slow-decaying MEPPs and desynchronized events

As already mentioned, about 14% of all MEPPs recorded in the *Torpedo* electric organ had an atypical slow rate of decay. In addition, we occasionally encountered signals that could hardly be categorized. They were suggestive of a marked disorganization of the release process. Some of them are illustrated in Fig. 7. The trace in Fig. 7*A* shows for comparison two fast-MEPPs, a sub-MEPP and a quantal-MEPP. In trace *B*, a slow-rising and slow-decaying MEPP exhibited several bumps on its rising phase. Another type of composite MEPP is illustrated in the record trace *C*. Such disorganized pictures were not of rare occurrence; they were sometimes encountered after a long silent period. We also encountered short bursts of sub-MEPPs (Fig. 7*D*), some of them were the size of a sub-MEPP, while the other ones were larger. Again, such bursts of sub-MEPPs often occurred isolated during a period of low frequency.

Computer analysis of the fast-MEPPs population

The two striking features found with the fast-MEPPs recorded from a patch area of *Torpedo* electroplaque were (i) the wide range of amplitude and (ii) the positive correlation of amplitude with both the time to peak and the half-decay time (Fig. 4). Three hypotheses were considered for explaining these observations. (a) External

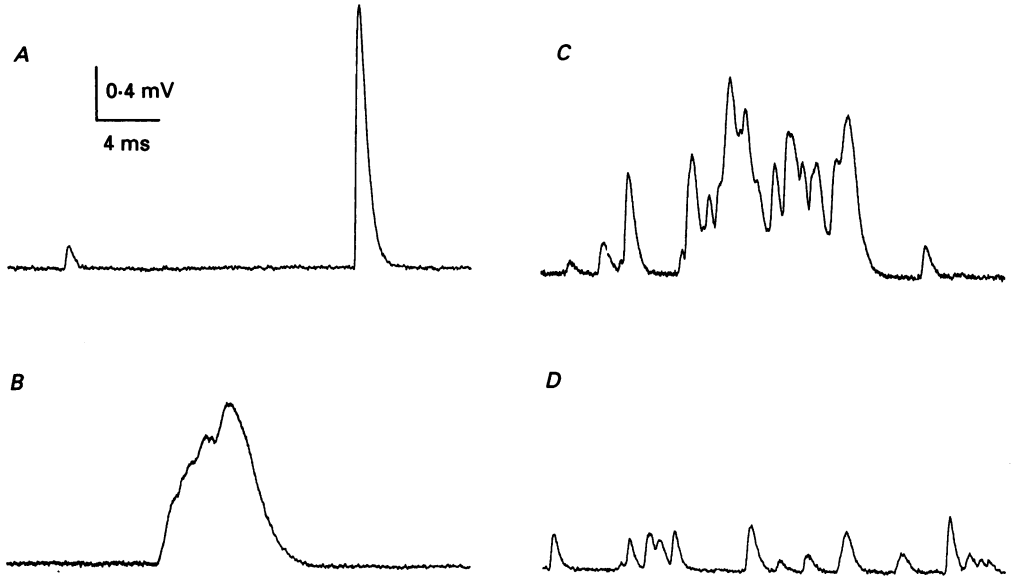

Fig. 7. Disorganized signals recorded in the electric organ. *A*, two consecutive fast-MEPPs, one sub-MEPP and one quantal-MEPP. *B*, a slow-rising and slow-decaying MEPP; note several bumps on the rising phase suggesting a substructure. *C*, high frequency burst of composite MEPPs in which individual sub-MEPPs co-exist with better synchronized signals. *D*, burst of events composed of individual sub-MEPPs.

MEPPs of small amplitude were MEPPs of quantal size generated at some distance from the patch; the signal recorded in the electrode was thereby attenuated. (b) Release of transmitter at a given spot in the patch was made at different ACh amounts (or of a different number of subunits). This could provoke a 'spatial interaction' in the postsynaptic activated fields, as investigated above for the evoked quanta. (c) The duration of ACh release lasted longer for the larger events (or the subunits were released successively at short time intervals).

Hypothesis (a) could be simulated by simply adding various values of resistance and capacity to a modelled signal of quantal size and time course. Addition of a resistance and a capacity did alter both the amplitude and the time course. However, the relationships computed between the amplitude and either the rise time or the decay time was the opposite of those found with the actually recorded fast-MEPPs. With space attenuation, the smaller an event, the longer its time course. Attenuation might nevertheless explain the occurrence of a small number of MEPPs of low amplitude displaying both a slow rise and a slow decay.

Hypothesis (b) was tested by using the theoretical model. A standard quantum was supposed to contain 10000 ACh molecules and to be composed of ten subunits,

each containing 1000 molecules. One to ten subunits were delivered synchronously at spots separated from each other by different distances (see Fig. 2). The result of the simulation is shown in Fig. 8 which illustrates the computed traces and the relationships obtained with one, five or ten subunits, emitted from sites separated by gaps of 600, 300 and 0 nm. Consider first the condition in which the release sites were

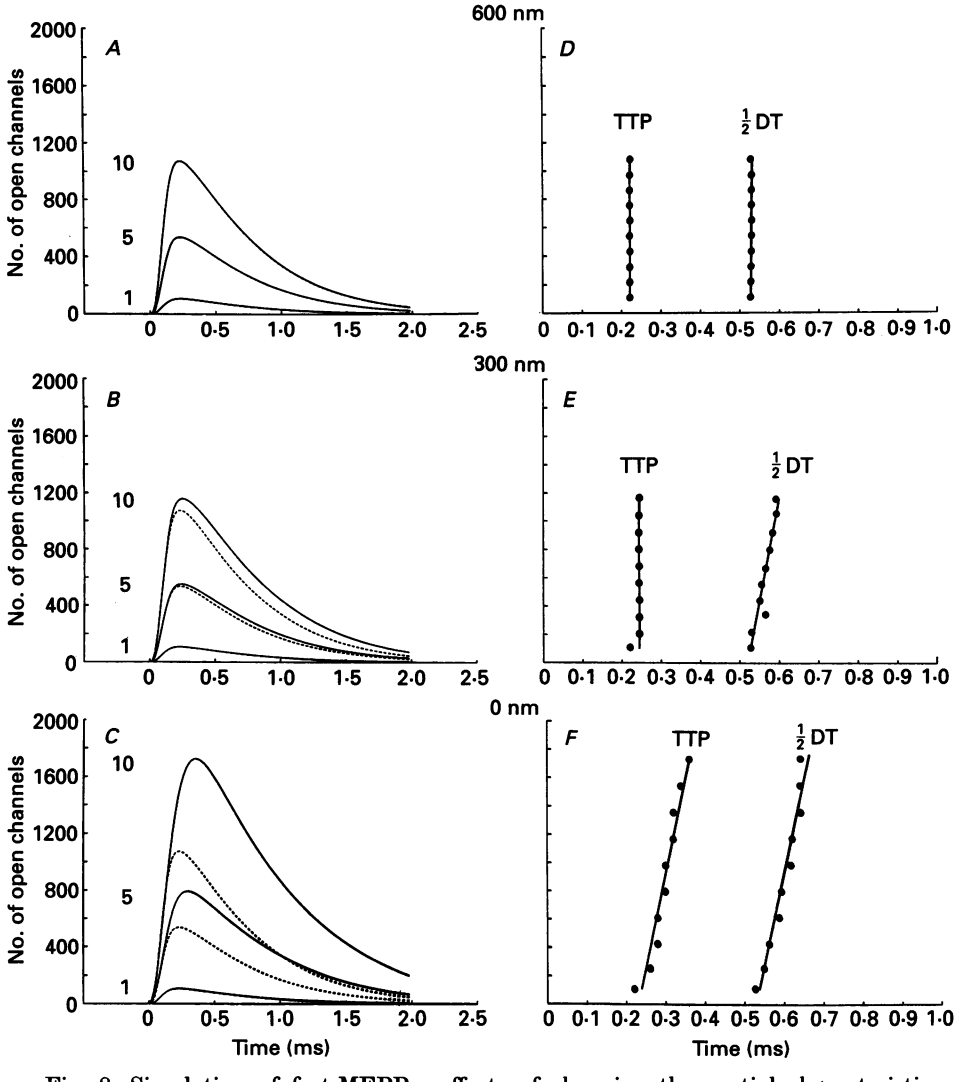

Fig. 8. Simulation of fast-MEPPs: effects of changing the spatial characteristics of transmitter release. One to ten packets of 1000 ACh molecules each were injected synchronously from sites separated by gaps of 600, 300 and 0 nm (conditions shown in Fig. 2). *A–C*, responses obtained after injection of 1, 5 and 10 packets; the dashed curves were calculated by multiplying by 5 or 10 the response to a single packet. *D–F*, plots with regression lines of amplitude *vs.* time to peak (TTP) and half-decay time ($\frac{1}{2}$ DT) of the responses to 1–10 packets. When injection sites were 600 nm apart (no overlap of receptor fields), responses were simply additive and the time course was independent of amplitude. When all subunits were delivered from the same point, a strong interaction potentiated the amplitude and prolonged the time course of the composite response.

situated at 600 nm from each other. The responses to an increasing number of subunits added linearly to each other and the simulated MEPPs of all sizes displayed a similar time course (Fig. 8*A*). There was consequently no correlation between time-to-peak and amplitude, and between half-decay time and amplitude (Fig. 8*D*). In contrast, when the subunits were emitted at a unique source (0 nm apart; Fig. 8*C* and *F*), both the amplitude and the time course of the composite responses markedly deviated from the figure expected from an additive process. The amplitude of the responses to five or ten subunits was much larger than five or ten times the amplitude of the response to a single subunit. Also the time course was changed since both the time to peak and the half-decay time exhibited a positive correlation with the amplitude (Fig. 8*F*).

A distance of 300 nm between the sites of subunit emission represented a threshold for this phenomenon; there was a small superadditivity of amplitude, little or no relationship between time to peak and amplitude, but a clear increase in the half-decay time with increased amplitude (Fig. 8*B* and *E*). The effects of reducing the gap between the subunit release sites were computed, as was done in Fig. 3 for quantal release (not illustrated). From comparison with the relationships found with the recorded fast-MEPPs, the model suggested that the different amounts of transmitter composing a MEPP should be emitted at spots disposed very close to each other, between 0 and 200 nm.

Hypothesis (c) proposed that the larger MEPPs had a slower time course because the subunits were released successively at short time intervals. This was tested by simulating desynchronized injection of one to ten subunits from release sites located 600 nm apart (see Fig. 9*A*). Desynchronization has three effects. First, the amplitude of the composite curves was smaller than calculated by additivity of the elementary response. Second, as expected, the larger responses displayed a longer time-to-peak. Third, the half-decay time of the simulated responses remained constant when the amplitude was increased (simulation not illustrated). The latter observation was in obvious contrast with the characteristics of physiological MEPPs whose half-decay time *increased* with amplitude. The same conclusion was reached whatever the interval of desynchronization, and whatever the distance separating the release sites from each other.

Computer simulation of slow-MEPPs

We first envisaged the possibility that changes in postsynaptic links could occur in given areas and produce atypically shaped signals. For this purpose, MEPPs were simulated by the release of quanta of 10000 ACh molecules on a single spot; this mode of emission was maintained constant, whereas the different postsynaptic parameters were systematically modified. The following changes caused prolongation of both the rising and the decaying phases of the simulated MEPP: (i) slowing down the ACh diffusion rate; (ii) reducing AChE activity by decreasing the number of active sites, the binding of ACh to the enzyme or the rate of hydrolysis; (iii) decreasing the rate of unbinding of ACh from the nicotinic receptors or the rate of closing of the channels. A reduction of ACh receptor density induced some lengthening of the rising phase, but caused the decay to be shortened and the amplitude to be strongly reduced. Finally, changing either the velocity of ACh binding to the receptor or the rate of channel opening did not modify the rising phase

in an appreciable manner. Traces obtained with these alterations of postsynaptic links were compared to the external MEPPs actually recorded from the preparation. A certain proportion of slow-decaying MEPPs could be imitated by manipulation of the postsynaptic links but the particular population of MEPPs exhibiting a slow rise

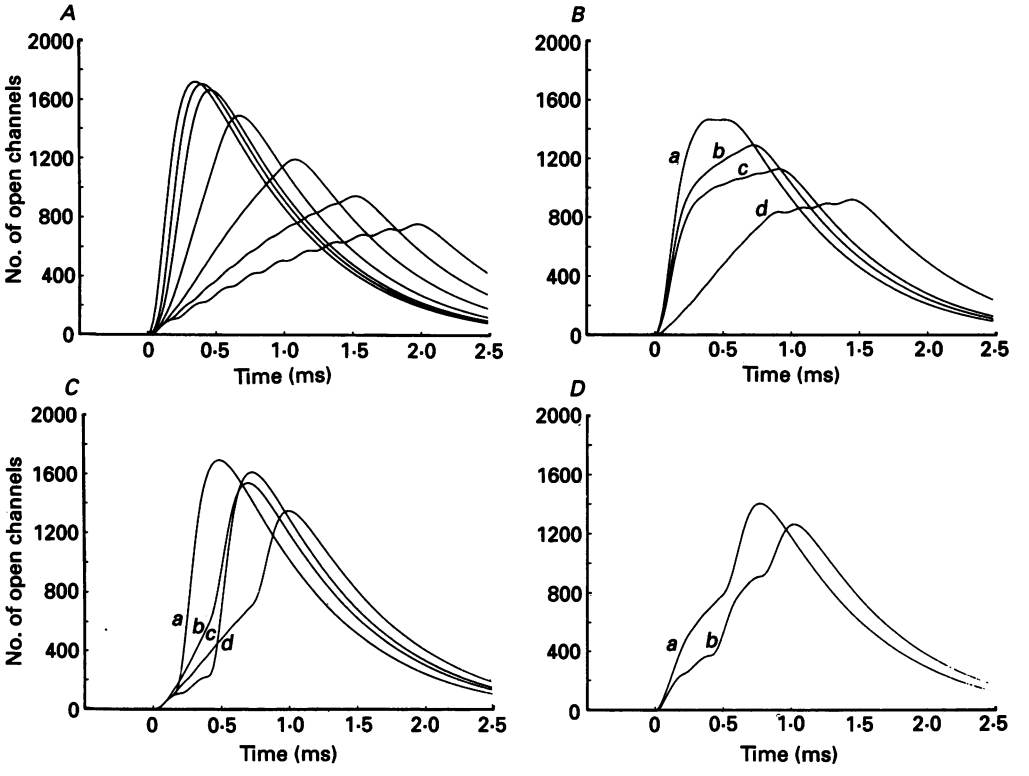

Fig. 9. Simulation of slow-rising MEPPs. *A*, successive emission, with even intervals of desynchronization, of 10 packets, each composed of 1000 ACh molecules. All subunits were injected on a single common spot of the simulated postsynaptic surface. The intervals of desynchronization were 0, 10, 20, 50, 100, 150 and 200 μs. *B*, simulated shoulder-MEPPs; the following patterns of subunit injections were: for curve *a*, 8 subunits in one shot, then 2 subunits at 200 μs intervals; *b*, 6 then 4 at 120 μs intervals; *c*, 5 then 5 at 150 μs intervals; *d*, 7 subunits at 120 μs intervals, then 3 at 180 μs intervals; *C*, simulated foot-MEPPs; for curve *a*, 1 subunit, followed 200 μs later by 9 subunits in one shot; *b*, 5 at 80 μs intervals, followed 80 μs later by 5; *c*, 2 at 200 μs intervals, followed 200 μs later by 8; *d*, 6 at 150 μs intervals, followed 150 μs later by 4; *D*, simulated MEPPs showing several inflexions on their rising rate; for curve *a*, one shot of 3 subunits, followed 120 μs later by 3 at 120 μs intervals, and one shot of 4 subunits 120 μs later; *b*, one shot of 2, then 1 subunit 200 μs later, 3 subunits 200 μs later, 1 subunit 180 μs later, 3 subunits 180 μs later.

but a rapid decay could not be reproduced in this way. Also the MEPPs exhibiting inflexions or bumps in their rising phase, as well as disorganized events (Fig. 7) could not be imitated by alteration of postsynaptic parameters.

On the other hand, any type of slow-rising MEPP could be easily simulated by changing with different patterns the kinetics of release during emission of an individual quantum. The first pattern consisted of delivering the ten subunits

successively with a fixed interval of desynchronization, from 10 to 200 μs. This resulted in simulated signals which resembled those MEPPs characterized by a slow but smooth rising phase (Fig. 9*A*).

We then introduced other patterns of subunit emission with abrupt changes at different times and found that the wide variety of slow-rising MEPPs encountered in the electric organ can be easily mimicked, including all types of foot-MEPPs and shoulder-MEPPs (Fig. 9). Shoulder-MEPPs were simulated by delivering at first the majority of subunits in a single discharge, followed by emission of the remaining subunits with various delays. The initial slope of the simulated trace was a function of number of subunits in the initial discharge (see curves *a*, *b* and *c* in Fig. 9*B*). The slopes of simulated shoulder-MEPPs before and after the break were systematically analysed in this way and the results fit well in the picture of the recorded shoulder-MEPPs described in Fig. 6*C* and *D*.

As for the foot-MEPPs, they were simulated by initial emission of one subunit, or of several successive subunits, followed after a delay by the synchronous discharge of the remaining subunits (Fig. 9*C*). Minimal value for the initial slope was the slope of a single subunit; with increasing synchronization during the foot, the subunit fused and the initial slope was consequently increased. After the foot, the rising slope became comparable to that of simulated quantal-MEPPs. Again, these observations met the histogram analysis of slopes presented in Fig. 6*E* and *F* for physiological foot-MEPPs.

Taken as a whole, the simulated slow-rising MEPPs produced by desynchronized emission of ACh subunits displayed signals of reduced amplitude and prolonged rising phase, whereas the decaying kinetics and the surface remained almost unaltered. This was in good accordance with the characteristics of the recorded slow-rising MEPPs.

Another observation was made from the curves shown in Fig. 9. With desynchronization intervals larger than 150 μs, that is, about 70% of the time to peak of a response to a single subunit (0·220 ms), waves revealing the individual subunits became apparent on the ascendent phase of the simulated curves. As already mentioned, similar oscillations were detected on the rising phase of several recorded slow-rising MEPPs (see Fig. 5). Finally, when subunits were produced with various patterns at larger time intervals, composite events like those of Fig. 7 were readily mimicked (not illustrated).

DISCUSSION

Postsynaptic currents at the nerve–electroplaque junction

Spontaneous and evoked transmitter release was analysed in a limited patch area of innervated membrane in which a maximum of ten to twenty quanta could be generated. Quantitative data were searched for by comparing the recorded traces with the predictions of a theoretical mode of synaptic transmission.

The rise of a postsynaptic current has been ascribed chiefly to three processes, that are: (i) ACh diffusion in the cleft; (ii) ACh binding to receptors, and (iii) receptor channel opening, with no step being rate limiting. Little attention was paid, however, in preceding studies to the rate of transmitter release itself.

The majority of evoked and spontaneous currents investigated in the present work exhibited a rapid rising phase. The mean MEPP time to peak was 0·44 ms and the rise time (from 20 to 80% of the peak maximum) was 0·19 ms. These values were shorter than those reported by Soria (1983) for the electric organ but it should be noted that both slow and fast signals were probably included in his investigation and that MEPPs of small amplitude were not recorded. On the other hand, the rising kinetics described here were very close to the values obtained from neuromuscular junctions of various species, where the rising time of spontaneous MEPCs ranges from 0·05 to 0·30 ms (Magleby & Stevens, 1972; Gage & McBurney, 1975; Land *et al.* 1981; Erxleben & Kriebel, 1988*a*).

The decay of *Torpedo* MEPPs was relatively rapid, with a mean half-decay time of 0·45 ms and a mean constant of decay of 0·35 ms. This was less than the corresponding values obtained in neuromuscular junctions (decay time constant ranging from 0·80 to 2·10 ms; Magleby & Stevens, 1972; Gage & McBurney, 1975; Land *et al.* 1981, 1984; Linder, Pennefather & Quastel, 1984; Erxeleben & Kriebel, 1988*a*). As already indicated, this discrepancy between the two synapses probably reflected a faster closing rate of the channel in the electric organ (Sakmann *et al.* 1985). The brief duration of the electrical current in this system might have a functional significance for a marine electric fish whose discharge is only composed of EPCs. Indeed, the efficiency of an electric shock is expected to be high at a minimal energy cost if the discharge is brief.

Postsynaptic areas activated by evoked multiquantal release

In well-synchronized responses, the time to peak of EPCs was not correlated with amplitude, but a positive relationship was observed between half-decay time and amplitude. Comparison with the model suggested that the quanta in the electric organ were released at a precise distance from each other, so that there was an interaction between the fields of activated receptors but this interaction only affected the late phase of the response. From this, the intervals separating the quantal release sites were estimated to range within 600 and 1000 nm in the electric organ (Figs 1 and 3). It was previously calculated that the maximum release rate in this synapse is 1·3 quanta per μm^2 (Dunant & Muller, 1986), corresponding to a mean space interval of 990 nm between quantal release sites. The value falls in the range predicted by the present approach. In the *Torpedo*, in which the electric discharge is the sum of pure EPCs, optimal use of synaptic space is apparently achieved with release sites disposed at a critical distance from each other, so that the quanta activate quasi-independent but adjacent postsynaptic areas. The present study also suggested that *ca* 10000 ACh molecules represent an optimal quantal content for efficiency of fast synaptic transmission. With larger amounts delivered from the same source, many molecules would be wasted without having an opportunity to activate receptors. This suggests that some regulation determines a precise relationship between the location of the release sites and the postsynaptic structures.

Amplitude and the time course of fast-MEPPs

The occurrence in electric organ of sub-MEPPs in addition to quantal-MEPPs (Muller & Dunant, 1987) resembled the pattern found at the endplate. It raised the question of whether the quantal-MEPP (and the evoked unitary EPP) is composed

of a number of discrete subunits (Kriebel & Gross, 1974; Matteson *et al.* 1981; Erxleben & Kriebel, 1988*b*). The subunit hypothesis was based on the observation of multiple peaks in both the small MEPP and the quantal-MEPP populations. Multiple peaks were often found in the distribution of small MEPPs in electric organ (Fig. 4*F*; see also Figs 1, 3, 4 and 5 in Muller & Dunant, 1987), but they were not clearly distinguished in the bell-shaped distribution of quantal-MEPPs. No systematic attempts to detect them were made in the present work.

The salient observation of this work was the relationship between the amplitude and the time course of spontaneous MEPPs: the larger the amplitude, the longer the time to peak and also the half-decay time. These relationships were found in the absence of acetylcholinesterase inhibitor, constantly in all preparations. To explain them, we proposed three hypotheses: (i) the small-MEPPs were attenuated signals arising from normal quanta generated at a remote distance from the electrode, for example in the subjacent electroplaques; (ii) MEPPs were composed of various amounts of transmitter (or of subunits) released close to each other and there was a dynamic overlap of the receptors' fields activated by each subunit; (iii) the observed relationships were ascribed to temporal factors: the subunits were delivered successively (or the release from one point source operated with an increased duration).

Hypothesis (i) (attenuation) and hypothesis (iii) (desynchronization) were both rejected when the actual fast-MEPPs were compared to the responses of the model. In contrast, the test of hypothesis (ii) (spatial interaction) gave simulated MEPPs very similar to the observed events and made it very likely that spatial interaction occurred during the generation of a quantum. The following description can be proposed; it is derived from the saturated disc model described by Salpeter and colleagues (Fertuck & Salpeter, 1976; Land *et al.* 1981, 1984; Bartol *et al.* 1991). When a given amount of ACh molecules are released from a single source, they activate a disc of receptors whose diameter increases as a function of time (see Fig. 2). In the centre of the disc most receptors are occupied by two ACh molecules but at the periphery, where the concentration of diffusing ACh is lower, there is a fringe of receptors to which only one molecule is bound. When two neighbouring fields are simultaneously activated in this way, an interaction arises from overlap of the fringes, increasing the probability for a number of receptors to be doubly bound. As a consequence the response to two subunits will be greater than to two times one subunit. The present study suggests that the different amounts of transmitter composing a MEPP, or the subunits, are released from sites less than 200 nm apart in this synapse, perhaps even from a unique source.

At the neuromuscular junctions no correlation between time to peak and amplitude was reported for spontaneous MEPCs recorded in the absence of anticholinesterase agent (Linder *et al.* 1984; Erxeleben & Kriebel, 1988*a*); but see Negrete, Del Castillo, Escobar & Yankelevich, 1972) whereas a positive correlation was observed upon AChE inhibition (Bevan, 1976; Land *et al.* 1981; Erxeleben & Kriebel, 1988*a*). As for the relation between MEPCs decay rate and amplitude in muscle with unblocked cholinesterase, some authors reported a positive correlation (Linder *et al.* 1984), while others did not (Lane *et al.* 1984; Erxleben & Kriebel, 1988*a*). These data suggest that in neuromuscular junctions ACh subunits do not

interact on the receptive surface when esterase is active, at least during the rising phase of MEPCs.

This perhaps explains why multiple peaks at regular intervals have been reported at the endplate (Kriebel & Gross, 1974; Matteson *et al.* 1981; Erxleben & Kriebel, 1988*b*) but were hardly distinguished in the amplitude distribution of *Torpedo* quantal MEPPs. Such peaks would be expected to occur at increasing intervals (and also with an increasing variance), making them difficult to detect.

Atypical miniature potentials at the neuromuscular and nerve–electroplaque junctions

There is some confusion in the classification of MEPPs, or MEPCs, of different kinds that have been recorded at the endplate. Oversized events, or 'giant-MEPPs', were first analysed by Liley (1957) who proposed that they were composed of two or several superposed normal MEPPs. Giant-MEPPs were later investigated more thoroughly by Thesleff & Molgó (1983) as well as their co-workers (see for a review Lupa, 1987). Giant-MEPPs were supposed to arise from a mechanism different from that responsible for the production of the usual quantal-MEPPs, since they are sensitive to different challenges and are not calcium dependent. The term 'slow-MEPPs' was attributed to events whose time course was altered, especially those with a prolonged time to peak (Lupa, 1987; Vautrin & Kriebel, 1991). In many circumstances the population of slow-MEPPs and that of giant-MEPPs increase in parallel. Thus both types share common properties. Giant-MEPPs were only exceptionally encountered in the present work probably due to the good insulation of the investigated area with the patch electrode.

A population of small MEPPs was termed 'sub-MEPPs' or 'skew-MEPPs' since they present themselves on amplitude distribution histograms as a distinct mode, skewed toward the background noise. Skew-MEPPs can be recorded only when the signal-to-noise ratio is appropriate. They have been found at the neuromuscular junctions of many species, in the electric organ of *Torpedo* as well as in other synapses (Kriebel & Gross, 1974; Muller & Dunant, 1987; Erxleben & Kriebel, 1988*a*, *b*).

'Quantal-MEPPs' or 'fast-MEPPs' apparently form the only population that can be released in a calcium-dependent manner on depolarization of nerve terminals. On the other hand, the production of sub-MEPPs, slow-MEPPs and giant-MEPPs is enhanced by a variety of manoeuvres in an unspecific and calcium-independent fashion (see Dunant, 1986). This prompted Vautrin & Kriebel (1991) to arrange all MEPPs into two general classes, the fast-MEPPs (including quantal-MEPPs) and the skew-MEPPs (including sub-MEPPs, slow-MEPPs and giant-MEPPs).

Slow-rising MEPPs and the possible subunit composition of the quantum

Slow-rising MEPPs had a mean constant of decay of 0·36 ms, like fast-MEPPs (0·35 ms). It seems, therefore, that all postsynaptic links operated normally at the places where slow-rising MEPPs were produced. Indeed, in our simulation, manipulations of AChE activity or of the number or the function of receptors, altered the decay phase of MEPPs to a greater extent than the rising phase. Another suggestion might be that slow-rising MEPPs arose from the coincidence of two or more quantal-MEPPs slightly out of phase. This was unlikely, however, since the amplitude of slow-rising MEPPs was on average lower than that of the quantal

population of fast-MEPPs; moreover, the proportion of slow-rising MEPPs was not increased during periods of high frequency.

For an alternative explanation for slow-rising MEPPs, we looked for a kinetic alteration of the release process itself. The subunit hypothesis seemed to be suitable for this purpose for the following reasons (see also Vautrin & Kriebel, 1991): (i) the occurrence of isolated sub-MEPPs in the present records, (ii) the inflexions and bumps observed in their rising phase of many slow-MEPPs, and (iii) the occurrence of bursts of sub-MEPPs and of the composite events revealing an obvious composite nature (Fig. 7).

In the generation of a slow-MEPP, it is proposed that the transmitter quantity normally mobilized for a quantal-MEPP is not delivered abruptly in one shot, but is released with an altered time course. By using the computer model it was just needed to desynchronize the release of subunits with various patterns to transform a fast-MEPP into a slow-rising MEPP of any kind. For a foot-MEPP, one or a few subunits have to be released first and then the rest of the quantum is delivered synchronously. A shoulder-MEPP would result from an initial discharge of the major part, followed by a delayed release of the resting subunits.

The number of subunits was made to vary around a preferential value (10 in our simulation). Any desynchronization of release in this case produced simulated signals whose amplitude was on average smaller than in the simulated fast-MEPPs, but whose decay kinetic was unaltered. All these properties were found with the actually recorded slow-rising MEPPs, however various their shape could be.

The change of slope affecting either shoulder-MEPPs and foot-MEPPs was revealing in this connection. The initial slope of shoulder-MEPPs was apparently rapid but precise measurements showed that it was on average significantly slower than in the mean quantal population. The model predicted that the initial slope would depend on the number of subunits delivered in the first shot. Thus, taking a preferential number of ten for the whole quantum and allowing a few subunits to be delayed, one has to conclude that the initial shot was on average composed of less than ten subunits, therefore that the initial slope was on average slower than in the quantal synchronized responses.

Relevance of the present findings to the mechanism of transmitter release

The present results raised several questions related to the cytological organization of neuromuscular and nerve–electroplaque transmission. Briefly summarized, our experiments on the electric organ supported the view that one quantum of transmitter was composed of subunits containing 1000 ACh molecules each. The number of subunits displayed some variation around a preferential value which appeared to be ten or so. The subunits were released either from a unique source or less than 0·2 μm apart. On the other hand, the quanta themselves were produced at slightly less than 1 μm from each other, so they activated just adjacent receptor fields. For the majority of spontaneous MEPPs and for almost all the evoked quanta, the subunits were discharged synchronously in a single shot. In quite a number of spontaneous MEPPs, however, subunits were released either isolated, or with the preferential grouping but not with a perfect synchronization.

Further work will be necessary to elucidate the role of synaptic vesicles in this system. The electric organ of *Torpedo* is the tissue above all from which the synaptic

vesicles have been isolated and characterized (see review in Israël, Dunant & Manaranche, 1979). Synaptic vesicles in the electric organ are much larger than those of the neuromuscular junction. They have been reported to contain approximately 200000 ACh molecules per vesicle (Ohsawa, Dowe, Morris & Whittaker, 1979). By supposing that transmitter release is supported only by exocytosis of synaptic vesicles of a smaller size, one would have enough ACh in each vesicle to make at least ten quanta. Additional mechanisms have to be imagined to account for the very precise substructure of the quantum, described in this report as well as at the neuromuscular junction (Vautrin & Kriebel, 1991).

A possibility is that synaptic vesicles do not completely fuse with the plasma membrane but would initially dock on it, and then transmitter release would be carried out by transport proteins that would channel ACh from the vesicle to outside. A cluster composed of a preferential number of such proteins could be responsible for the production of one quantum. One vesicle would therefore serve for the generation of several quanta. The mediatophore could be involved in this process. The mediatophore is a protein purified from the plasma membrane of cholinergic nerve terminals. When reconstituted into liposomes or into *Xenopus* oocytes, it endows them with the ability to release ACh in a Ca^{2+}-dependent manner (Birman, Israël, Lesbats & Morel, 1986; Cavalli, Eder-Colli, Dunant, Loctin & Morel, 1991). Alternatively, a cluster of mediatophores could make use of cytosolic ACh and release it into the synaptic space directly. This would be in line with the observation that cytosolic ACh is apparently the pool most immediately available for release in the electric organ *in situ* and in isolated synaptosomes (see Israël *et al.* 1979; Dunant, 1986).

In the electric organ when a nerve impulse is transmitted, the number of large intramembrane particles abruptly increases for 2–3 ms in the presynaptic plasmalemma; sometimes these particles group to form a double row pattern resembling that of resting mammalian endplates (Fig. 3 in Muller, Garcia-Segura, Parducz & Dunant, 1987). It is of course tempting to suggest that this may be the fleeting image of quantal release by a group of mediatophores. The question of subunit synchronization is intriguing. It could be explained by ten or so mediatophores operating under the control of a calcium-sensitive synchronizing protein (see Dunant, 1986). Another possibility would be that the mediatophores are grouped around a calcium channel. This would explain why the subunits are apparently better synchronized in the evoked EPC, when calcium ions have to enter the membrane for triggering the release. These proposals are of course speculations at the present time, but any model of the release process will have to account for the observation that the quantum exhibits a fine dynamic substructure.

This work was supported by grant no. 31-28780.90 of the Swiss FNRS. We are grateful to D. Muller for fruitful suggestions, to S. Bonnet, N. Collet, F. Loctin, F. Pillonel, J. Richez and J. C. Vincent for help during the course of the work and manuscript preparation.

REFERENCES

ADAMS, P. R. (1981). Acetylcholine receptor kinetics. *Journal of Membrane Biology* **58**, 161–174.

ANDERSON, C. R. & STEVENS, C. F. (1973). Voltage clamp analysis of acetylcholine produced end-plate current fluctuations at frog neuromuscular junction. *Journal of Physiology* **235**, 655–691.

BARTOL, T. M., LAND, B. R., SALPETER, E. E. & SALPETER, M. M. (1991). Monte Carlo simulation of miniature end-plate current generation in the vertebrate neuromuscular junction. *Biophysical Journal* **59**, 1290–1307.

BENNETT, M. V. L., WURZEL, M. & GRUNDFEST, H. (1961). Properties of electroplaques of *Torpedo nobiliana*. *Journal of General Physiology* **44**, 757–804.

BEVAN, S. (1976). Sub-miniature end-plate potentials at untreated frog neuromuscular junctions. *Journal of Physiology* **258**, 145–155.

BIRMAN, S., ISRAËL, M., LESBATS, B. & MOREL, N. (1986). Solubilization and partial purification of a presynaptic membrane protein ensuring calcium-dependent acetylcholine release from proteoliposomes. *Journal of Neurochemistry* **47**, 433–444.

CAVALLI, A., EDER-COLLI, L., DUNANT, Y., LOCTIN, F. & MOREL, N. (1991). Release of acetylcholine by *Xenopus* oocytes injected with mRNAs from cholinergic neurons, *EMBO Journal* **10**, 1671–1675.

COLQUHOUN, D. & OGDEN, D. C. (1988). Activation of ion channels in the frog end-plate by high concentrations of acetylcholine. *Journal of Physiology* **395**, 131–159.

COLQUHOUN, D. & SACKMANN, B. (1985). Fast events in single channel currents activated by acetylcholine and its analogues at the frog muscle end-plate. *Journal of Physiology* **369**, 501–507.

COUTEAUX, R. & PÉCOT–DECHAVASSINE, M. (1973). Données ultrastructurales et cytochimiques sur le mécanisme de libération de l'acétylcholine dans la transmission synaptique. *Archives Italiennes de Biologie* **3**, 231–262.

DUNANT, Y. (1986). On the mechanism of acetylcholine release. *Progress in Neurobiology* **26**, 55–92.

DUNANT, Y. & MULLER, D. (1986). Quantal release of acetylcholine evoked by focal depolarization at the *Torpedo* nerve–electroplaque junction. *Journal of Physiology* **379**, 461–478.

ERXLEBEN, C. & KRIEBEL, M. E. (1988*a*). Characteristics of spontaneous miniature and subminiature end-plate currents at the mouse neuromuscular junction. *Journal of Physiology* **400**, 645–658.

ERXLEBEN, C. & KRIEBEL, M. E. (1988*b*). Subunit composition of the spontaneous miniature end-plate currents at the mouse neuromuscular junction. *Journal of Physiology* **400**, 659–676.

FERTUCK, H. C. & SALPETER, M. M. (1976). Quantitation of junctional and extrajunctional acetylcholine receptors by electron microscope autoradiography after ^{125}I-α-bungarotoxin binding at mouse neuromuscular junctions. *Journal of Cell Biology* **69**, 144–158.

GAGE, P. W. & MCBURNEY, R. N. (1975). Effects of membrane potential, temperature and neostigmine on the conductance change caused by a quantum of acetylcholine at the toad neuromuscular junction. *Journal of Physiology* **244**, 385–407.

HARTZELL, H. C., KUFFLER, S. W. & YOSHIKAMI, D. J. (1975). Post-synaptic potentiation: interaction between quanta of acetylcholine at the skeletal neuromuscular synapse. *Journal of Physiology* **251**, 427–463.

HEUSER, J. E. & SALPETER, S. R. (1979). Organization of acetylcholine receptors in quick-frozen, deep etched, and rotary-replicated torpedo postsynaptic membranes. *Journal of Cell Biology* **82**, 150–173.

ISRAËL, M., DUNANT, Y. & MANARANCHE, R. (1979). The present status of the vesicular hypothesis. *Progress in Neurobiology* **13**, 237–275.

KATZ, B. (1969). The release of neural transmitter substances. *The Sherrington Lectures*, vol. X. Liverpool University Press, Liverpool, UK.

KATZ, B. & MILEDI, R. J. (1973). The binding of acetylcholine to receptors and its removal from the synaptic cleft. *Journal of Physiology* **231**, 549–574.

KRIEBEL, M. E. & GROSS, C. E. (1974). Multimodal distribution of frog miniature end-plate potentials in adult, denervated, and tadpole leg muscle. *Journal of General Physiology* **64**, 85–103.

KUFFLER, S. W. & YOSHIKAMI, D. J. (1975). The number of transmitter molecules in a quantum: an estimate from iontophoretic application of acetylcholine at the neuromuscular synapse. *Journal of Physiology* **251**, 465–482.

LAND, B. R., HARRIS, W. V., SALPETER, E. E. & SALPETER, M. M. (1984). Diffusion and binding constants for acetylcholine derived from the falling phase of miniature end-plate currents. *Proceedings of the National Academy of Sciences of the USA* **81**, 1594–1598.

LAND, B. R., SALPETER, E. E. & SALPETER, M. M. (1981). Kinetic parameters for acetylcholine interaction in intact neuromuscular junction. *Proceedings of the National Academy of Sciences of the USA* **78**, 7200–7204.

LILEY, A. W. (1957). Spontaneous release of transmitter substance in multiquantal units. *Journal of Physiology* **136**, 595–605.

LINDER, T. M., PENNEFATHER, P. & QUASTEL, D. M. J. (1984). The time course of miniature end-plate currents and its modification by receptor blockade and ethanol. *Journal of General Physiology* **83**, 435–468.

LUPA, M. T. (1987). Calcium-insensitive miniature end-plate potentials at the neuromuscular junction. *Synapse* **1**, 281–292.

MADSEN, B. W., EDESON, R. O. & MILNE, R. K. (1987). Neurotransmission parameters estimated from miniature end-plate current growth phase. *Brain Research* **402**, 387–392.

MAGLEBY, K. L. & STEVENS, C. F. (1972). A quantitative description of end-plate currents. *Journal of Physiology* **223**, 173–197.

MATTESON, D. R., KRIEBEL, M. E. & LLADOS, F. (1981). A statistical model indicates that miniature end-plate and unitary evoked potentials are composed of subunits. *Journal of Theoretical Biology* **90**, 337–363.

MULLER, D. & DUNANT, Y. (1987). Spontaneous quantal and subquantal transmitter release at the torpedo nerve–electroplaque junction. *Neuroscience* **20**, 911–921.

MULLER, D., GARCIA-SEGURA, L. M., PARDUCZ, A. & DUNANT, Y. (1987). Brief occurrence of a population of presynaptic intramembrane particles coincides with transmission of a nerve impulse. *Proceedings of the National Academy of Sciences of the USA* **84**, 590–594.

NEGRETE, J., DEL CASTILLO, J., ESCOBAR, I. & YANKELEVICH, G. (1972). Correlation between amplitudes and rise times of the miniature end-plate potentials in frog muscle. *International Journal of Neuroscience* **4**, 1–10.

NIGMATULLIN, N. R., SNETKOV, V. A., NIKOL'SKII, E. E. & MANGAZANIC, L. G. (1988). Analysis of a model of the miniature end-plate current. *Neirofiziologiia* **20**, 390–398.

OHSAWA, K., DOWE, G. H. C., MORRIS, S. J. & WHITTAKER, V. P. (1979). The lipid and protein content of cholinergic synaptic vesicles from the electric organ of *Torpedo marmorata* purified to constant composition: implications for vesicle structure. *Brain Research* **161**, 447–457.

ROSENBERRY, J. (1975). Acetylcholine esterase. *Advances in Enzymology and Related Areas of Molecular Biology* **43**, 103–218.

SAKMANN, B., METHFESSEL, C., MISHINA, M., TAKAHASHI, T. & TAKAI, T. (1985). Role of acetylcholine receptor subunits in gating of the channel. *Nature* **318**, 538–543.

SALPETER, M. M., ROGERS, A. W., KASPRZAK, H. & MCHENRY, F. A. (1978). Acetylcholinesterase in the fast extraocular muscle of the mouse by light and electron microscope autoradiography. *Journal of Cell Biology* **78**, 274–285.

SORIA, B. (1983). Properties of miniature post-synaptic currents at the *Torpedo marmorata* nerve–electroplaque junction. *Quarterly Journal of Experimental Physiology* **68**, 189–202.

THESLEFF, S. & MOLGÓ, J. (1983). A new type of transmitter release at the neuromuscular junction. *Neuroscience* **9**, 1–8.

VAUTRIN, J. & KRIEBEL, M. E. (1991). Characteristics of slow-miniature end-plate currents show a subunit composition. *Neuroscience* **41**, 71–88.

WATHEY, J. C., NASS, M. M. & LESTER, H. A. (1979). Numerical reconstruction of the quantal event at nicotinic synapses. *Biophysical Journal* **27**, 145–164.